Mechanisms of Excitation and Remodeling of the Cardiac Action Potential in Two Model Systems

by

Ryan Peter O'Connell

A dissertation submitted in partial fulfillment
of the requirements for the degree of
Doctor of Philosophy
(Molecular and Integrative Physiology)
in the University of Michigan
2014

Doctoral Committee:

Assistant Professor Justus M. Anumonwo, Chair
Associate Professor Anatoli Lopatin
Associate Professor Daniele E. Michele
Associate Professor Mark W. Russell
Associate Professor Santiago D. Schnell

“…the problems of the human heart in conflict with itself, which alone can make good writing because only that is worth writing about, worth the agony and the sweat...”

William Faulkner, 1950

Dedicated to my amazing family. Without their love and support this work would not have been possible.

Acknowledgements

Reaching this milestone could not have been achieved without the support and guidance of many individuals at the University of Michigan. I am forever indebted to my mentor, Dr. Justus Anumonwo. His enthusiasm and direction has benefited me greatly as a scientist and has translated over into making me a better person. I truly appreciate his patience and wit in my development over the last number of years. I cannot express enough gratitude for all of the assistance and mentorship he has provided since I first joined his lab.

Thank you to my committee members, Drs. Anatoli Lopatin, Daniel Michele, Mark Russell, and Santiago Schnell. Your scientific insight during the maturation of my projects is greatly appreciated. I would also like to thank the Department of Molecular and Integrative Physiology for their support during my graduate career. I would like to specifically thank Michele Boggs. Over the course of my graduate career she has been nothing short of amazing in her assistance and guidance.

I owe a special thank you to the Center for Arrhythmia Research and specifically Drs. Jose Jalife and Hector Valdivia for providing such a challenging and nurturing environment in which to absorb basic cardiac electrophysiology. Two individuals who played a significant role in my development, Drs. Hassan Musa and Jerome Kalifa, deserve more recognition and thanks than I could ever provide in this space. They were unyielding in their support of my work and I feel

very fortunate to have had their personal and scientific guidance during graduate school.

I would like to thank Drs. Ravi Vaidyanthan and Makarand Deo for their assistance in completing the first project of this thesis. Completing a project in sheep is no small task. I would not have been able to perform any experiments if it wasn't for the contributing efforts of a number of individuals. I'd like to thank Drs. Steve Ennis, Rafael Ramirez, Uma Mahes Avula, Jerome Kalifa, Jiang Jiang and Raphael Martins for their contributions in teaching and assisting me in performing thoracotomies on large mammals. I would also like to thank a few members of the Center for Arrhythmia Research who I am indebted to for their scientific assistance and for simply being great people to study alongside: Drs. Todd Herron, Guadalupe Guerrero-Serna, Kuljeet Kaur, Michelle Milstein, Alexandra Bizy, David Auerbach, Ravi Vaidyanathan, Matt Klos, Katherine Campbell Luqia Hou, Vandana Verma and Cicero Willis. I would also like to specially thank Nulang Wang. Without her daily assistance there is no chance any of the projects I was involved with would have been completed. I am sincerely indebted to her for all of her help during my time at the Center for Arrhythmia Research.

Table of Contents

List of Figures

List of Tables

Abstract

Differences in cardiac ionic currents underlie action potential duration (APD) heterogeneity and alterations of any current may be arrhythmogenic. Biophysical analysis of ionic currents is crucial in understanding electrophysiological mechanisms of regional electrical heterogeneity and underlying factors that promote arrhythmogenicity.

The first project presented in this dissertation characterized, for the first time, the electrophysiology of the Purkinje system of the murine heart. Current-clamp analysis of Purkinje cells (PCs) demonstrated pacemaker activity and a prolonged plateau phase compared to ventricular myocytes (VMs). We investigated, using voltage-clamp, the major ionic currents underlying the action potential and automaticity in PCs and VMs. We observed hyperpolarization activated currents, which contribute to automaticity in PCs, but not VMs. PCs demonstrated differences in transient outward potassium currents, sodium current and T-type calcium current, which was not present in VMs. A computational model of the mouse PC was developed and simulations determined that unlike VMs, in PCs the presence of T-type calcium current was capable of prolonging APD.

The second project of this dissertation investigated the remodeling of action potentials in atrial cells by free fatty acids (FAs), which has not been investigated in large mammals. This project used an ovine model to serve as a better surrogate of human cardiac structure, electrophysiology and metabolism. Current-clamp analysis of ovine left atrial (LA) myocytes exposed to each of the major FAs showed that only stearic acid (SA) altered LA APD at all values measured. Voltage-clamp recordings showed a ~60% and ~30% reduction of I_{CaL} and I_{TO} in SA-treated cells. Integration of the experimental data into a computational model of the human atrial action potential showed reduction of I_{CaL} was sufficient to remodel LA APD. Reduction in I_{CaL} in SA-treated cells was accompanied by disruption of transverse (t)-tubules, a membrane compartment in which calcium channels are predominantly located into microdomains, thus providing a novel mechanism of cellular remodeling by fatty acids.

These two studies provide insight into ionic remodeling and importance of calcium currents in heterogeneity and alterations of the cardiac action potential.

Chapter 1

1.1 Thesis Introduction

The objective of this dissertation is to investigate the ionic basis of the cardiac action potential under physiological and pathophysiological conditions. The rhythmic generation and termination of the cardiac impulse is the fundamental principle governing proper contraction of the heart and is essential in maintaining blood flow to the cardiovascular system.

This thesis investigated, for the first time, the electrophysiological characteristics of Purkinje cells of the wildtype mouse heart. Purkinje cells (PCs) comprise the specialized conduction system of the ventricles and aid in rapidly transmitting the electrical impulse from the atria to the cardiac apex. PCs were identified by their distinct cellular morphology and the presence of spontaneous action potentials. Compared to ventricular myocytes (VMs), PCs had reduced membrane capacitance, which was consistent with smaller cell dimensions and the absence of transverse(t)-tubules. Current clamp analysis of PCs demonstrated significantly longer action potential durations (APD) compared to apical and septal myocyte APDs ($p<0.05$). Furthermore, isolated PCs exhibited pacemaker activity and early afterdepolarizations, which was not observed in either type of VM. Voltage clamp experiments focused on the primary ionic currents responsible for the action potential and pacemaker activity in the murine

model (I_f, I_{K1}, I_{TO}, I_{CaT}, I_{CaL} & I_{Na}). We integrated our experimental data into numerical simulation to gain further insight into the ionic mechanisms of the mouse PC. We developed a morphologically realistic simulation of the mouse PC integrating the experimental electrophysiological data and a radial spatiotemporal Ca^{2+} diffusion process between subsarcolemmal and subsarcoplasmic reticulum compartments. In these simulations, only the presence of the T-type calcium current was capable of prolonging the APD in PCs. The electrophysiological characterization of mouse cardiac PCs offers new possibilities to investigate the role of the conduction system in the generation and maintenance of inherited cardiac arrhythmias.

The primary advantage of the mouse model is that it may be genetically tailored to serve as a surrogate for human genetic diseases. However, the limitation of the mouse model became apparent as I began to undertake resolving the recently discovered association between increased epicardial fat in obese patients and atrial fibrillation. Particularly, the region of adiposity near the posterior left atrium (LA), which is both the site of increased adiposity in obesity and reentrant activity in atrial fibrillation. Mice, unlike humans or other large mammals, have little to no epicardial fat. Therefore, I had to implement an animal model with a metabolic profile, and epicardial fat distribution similar to humans. I transitioned my experiments from the murine to the ovine model. In this system, I investigated the effects of free fatty acids, which are elevated significantly during obesity, and their effects on left atrial (LA) myocyte electrophysiology. Very little is known about chronic exposure of myocytes to saturated fatty acids, a major

component of ovine epicardial adiposity. I investigated adipocyte paracrine modulation of cardiac myocytes and determined that saturated free fatty acids, particularly stearic acid, profoundly shortens LA APD. Voltage clamp recordings determined a 60% decrease of $I_{CaLpeak}$ current in stearic acid treated cells compared to vehicle controls. There were no differences in I_{Na} between control and stearic acid treated cells. We integrated the ionic current data into a previously published human atrial cell computational model and it recapitulated the experimentally observed reduction of the APD in cells incubated with stearic acid. To determine the mechanism by which the calcium current is reduced, we stained cells with Di-8-ANEPPS and determined that in cells incubated with stearic acid almost all t-tubules are not present. This finding suggests that loss of the t-tubule ultrastructure is responsible for the reduction of I_{CaL} and the shortening of the APD. The data collected here may serve as a link between the elevated risk of atrial fibrillation in obese patients and the underlying arrhythmogenic remodeling, which may provide novel therapeutic tfor patients in the future.

The overall hypothesis of this dissertation is that the heterogeneous nature of cardiac APD and the remodeling of the APD that occurs in pathophysiological conditions are the result of (1) differential ionic densities and channel expression and (2) the localization of ion channels to microdomains are another mechanism by which electrical excitation can be modulated.

1.2 Cardiac Structure and Electro-Mechanical Function

Introduction

The heart is a muscular pump responsible for propelling blood through arteries and veins via synchronized and rhythmic contractions. Movement of blood through the circulatory system delivers homeostatic biofactors, nutrients, removes waste products and is essential for the survival of all vertebrate organisms. An electrical impulse is responsible for controlling cardiac tissue contractions and impulse generation, propagation and termination will be discussed further in the “Cardiac Electrical Activity” and “Excitation-Contraction Coupling” sections. This section focuses on gross, cellular and molecular structures of the heart involved in mechanical force production.

1.2.1 Atrial Myocardium

The atria are thin-walled muscular chambers responsible for collection of venous blood from either the pulmonary (left) or systemic (right) circulation and for filling each ventricular chamber, respectively. Initiation of atrial contraction is controlled by a region of specialized cells, known as the sinoatrial (SA) node, located in the right atrium. The atria contain a second important grouping of specialized cells known as atrioventricular (AV) node. The AV node is responsible for electrically connecting the atria and ventricles as the cardiac

skeleton acts as an electrical insulator between the two regions. In addition, the AV node is responsible for generating a brief but important delay in the transmission of the electric impulse between the two regions. This delay allows for maximum filling of the ventricular chambers and reduces backflow into the atria. Atrial walls contain “ridges” called pectinate muscles, which are believed to contribute to preferential conducting pathways that link the SA and Atrioventricular (AV) nodes[8,9]. The region of the heart that encompasses the atrioventricular valves (and usually one semilunar valve) is referred to as the “base” of the heart. It was given this name due to the heart’s inverted cone or pyramid shape that extends towards its narrowest region (inferiorly from the base) referred to as the apex.

1.2.2 Ventricular Myocardium

The ventricular myocardium is considered the majority of ventricular tissue between the ventricular epicardium and endocardium. It consists of muscle fibers arranged in a latticework arising from the cardiac skeleton and spiraling towards the apex[10]. Interestingly, the muscle fibers at the epicardial surface of the left ventricle tend to be oriented perpendicularly to the base-apex axis, whereas muscle fibers at the endocardial surface tend to be more circumferentially oriented as shown in Streeter et al[11]. Analysis of fiber-shortening patterns during contractions of the left ventricular wall suggests the ventricle operates as a series of concentric shells that thicken as they contract, undergoing only minor angular distortions[12]. Ventricular walls are significantly thicker than those of the atria due

to an abundance of muscle fibers, which allows the ventricular chambers to develop higher pressures than the atria during contraction. This is necessary to overcome the resistance of the pulmonic and systemic circulations. This results in the left ventricle being three times the mass and twice the thickness of the right ventricle. The ventricular septum, a thick central portion of the ventricles that separates the two chambers, typically functions as part of the left ventricle by moving toward the left ventricular free wall during contraction. However, in certain pathological conditions such as pulmonary hypertension, the septum transitions to assist the right ventricle during contractions.

1.2.3 Specialized Conduction System (Purkinje Fibers)

In the 19th century a Czech phenomenologist, Johnannes Purkinje, was the first to describe the subendocardial fibers of the heart and due to his discovery these fibers bare his namesake[13]. However, at the time Purkinje incorrectly categorized these fibers as cartilage and it wasn't until 60 years after his initial discovery that Tawara et al demonstrated the electrical connection between the AV bundle and Purkinje fibers was essential to the propagation of the electrical impulse to the ventricles[14]. The Purkinje network extends from the central part of the cardiac skeleton at the AV Node inferiorly through the septum and along the subendocardial surfaces of the ventricles. The fibrous cardiac skeleton not only serves as structural support for the valves, but as an electrical insulator between the atria and ventricles. The skeleton "forces" the activation signal from the atria to be "collected" at the AV Node and transmitted through the

Purkinje fibers before activating the ventricular myocardium. Conduction through the Purkinje fibers allows for the initiation of ventricular contractions to originate at the apex and spread superiorly towards the base. This pathway of activation allows for maximum ejection of blood from the ventricles. Many ventricular arrhythmias are initiated in the Purkinje conduction system[15-17]. Both reentrant triggered and enhanced automatic rhythms can arise from the Purkinje fiber network in the presence of acquired diseases or gene-based channelopathies.

Purkinje cells are considerably different from ventricular cells at both the histologic and ultrastructural levels. Histologically, Purkinje cells stain lightly, due to the reduced myofibrillar content and enhanced glycogen compared to ventricular myocytes. Electron micrographs show Purkinje cells lack t-tubules and core dyad[18]. Recent immunostaining studies have confirmed distinguishable Purkinje cell-to-cell junctions and the existence of connexin40 (Cx40) protein as the major Purkinje connexin isoform[19]. Purkinje cells have traditionally been defined by lacking a complex t-tubule structure. It has been suggested that the presence of t-tubules may adversely affect the conduction velocity and thus may be a hindrance rather than a benefit for Purkinje fibers rapid conduction of electrical signals[18]. Purkinje cell morphology has been described in a variety of species and divided into three groups[20]. Group 1 is the Purkinje fiber network in sheep and goats, which had strands of 2-8 oval cells with relatively large deposits of connective tissue surrounding each fiber[21]. Purkinje cells in this group are much larger than ventricular myocytes, oval and connected with end-to-end or side-to-side contacts. Given the large surface area (and large gap junction

proteins) between each connecting Purkinje cell in group 1, the Purkinje network in group 1 is considered to have efficient conduction properties [22]. Purkinje cells in Group 2, which belong to human and canine are usually defined as cylindrical, running in parallel and making end-to-end contacts at intercalated discs. These morphological features suggest longitudinal propagation is the main path of conduction. Group 3, which represents mice and rats, Purkinje cells were very similar in appearance to ventricular myocytes. Purkinje cells in the present study were considerably smaller in size than ventricular myocytes[20]. The variation of each group may reflect the conducting function of the network in each species, respectively.

Electrophysiologically, Purkinje cells have been shown to have longer action potentials than neighboring ventricular myocytes[23]. In rabbit, Purkinje cells exhibit a prominent phase 1 repolarization, a more negative plateau, and a significantly longer final repolarization (APD90) than ventricular cells[24,25]. Similarly, in canine Purkinje fibers, APD50 and APD90 (percent repolarization from peak depolarization) are prolonged compared to ventricular myocytes [26-29]. However, the total amplitude of the action potential (APA) and the maximal rate of rise of the action potential upstroke (V_{max}) are much larger in Purkinje fibers versus the ventricle. Purkinje cells are also known to have two distinct calcium currents, which has been suggested to play a role in spontaneous activity (isoforms are discussed in subsequent sections)[30]. The successful electrophysiological characterization of Purkinje cells murine system has remained elusive due to the difficulty in the isolation procedure. Chapter 2 of this

dissertation aims to understand the underlying mechanisms of excitation in Purkinje cells of the mouse and to aid in the development of a numerical model to better understand sub-sarcolemmal calcium handling in the absence of t-tubules.

1.2.4 Myocyte ultrastructure

The cellular composition of the heart is divided into 5 major categories: myocytes, fibroblasts, endothelial cells, smooth muscle cells and adipocytes. The relative composition of each cell type varies with species but overall myocytes, the force generating cells of the myocardium, account for less than half of the cellular population of the heart[31]. However, myocytes are a significant majority of cellular mass of the heart. Histological studies revealed a striated latticework composed of sarcomeres, the force generating structures of myocytes across all myocyte types[32]. The presence of sarcomeres, shown in Spotnitz et al[32], gives myocytes their characteristic light and dark striations. The more darkly stained regions are due to the presence of tightly packed thick filaments composed of the protein myosin. Thick filaments rotate polarized light due to their highly ordered parallel array (anisotropy) and therefore designated A-bands. The lightly stained striations are more isotropic, designated I-bands, and contain the protein actin. Heavy and light filaments are anchored to structures, known as Z discs, primarily by the proteins Titin and CapZ, respectively. Z discs designate the terminal ends of one functional sarcomere and are formed primarily by α-actinin. A functional sarcomere generates contractile force by the interaction of myosin and actin

through myosin “cross bridges” formed by the proteins tropomyosin and troponin complex on the myosin filament. During systole, the thin filaments are drawn toward the center of the sarcomere by connection and movement of the tropomyosin and troponin complex. The molecular pathway and structures concerning sarcomere force generation and relaxation will be discussed further in the “Excitation-Contraction Coupling” (EC coupling) section. Additionally, histologic and electron micrograph studies determined a large fraction of the myocyte cell volume is occupied by mitochondria, which are responsible for generating chemical energy required for contraction. Taken together, the contractile proteins and mitochondria account for ~80% of the myocardial cell volume with the other major structures accounting for smaller fractions: cytosol (~10%), sarcoplasmic reticulum (~3%), transverse tubule network (~3%) and the nuclei (~2%)[33].

1.3 Cardiac Electrical Activity

1.3.1 Cardiac Impulse Initiation and Propagation

Contraction of the myocardium is the result of a carefully synchronized and rhythmic change in the electric potential of the heart beginning in a specialized zone of the right atrium (RA). This group of specialized myocytes represents a region of the heart that displays self-generating oscillations in membrane voltage that lead to the firing of action potentials (APs). This region is known as the sinoatrial (SA) node or the cardiac pacemaker and is located near the junction of the RA and superior vena cava (SVC). Interestingly, the exact

location and size of the SA node has considerable inter- and intra-species dependent differences that to this day are not entirely understood.

The electrical impulse from the SA node propagates across the RA, into left atria (LA) and arrives at the atrioventricular (AV) node as shown in Figure 1.3.1 (left panel). The AV node is located at the central junction between the atria and the ventricles. Furthermore, the AV node is responsible for generating a delay in the electrical impulse, due to slowing conduction, allowing the atria to fully contract and eject blood into the relaxed ventricles. Following this delay (~20-30 msec), the impulse then travels rapidly through the His bundle, the left and right bundle branch (LBB and RBB), and then finally through the extensive Purkinje (PKJ) network to initiate the synchronous contraction of the ventricles. The activation, location, directionality and termination of the electrical impulse as it propagates across the myocardium is responsible for the electrical signal monitored on a standard electrocardiogram (ECG) shown in Figure 1.3.1 (lower right panel). The variety of AP morphology shown in Figure 1.3.1 (right panel) across different regions of the heart have been attributed primarily to the diversity of ion channel expression patterns in each cell type.

1.3.2 Cardiac Action Potential

The myocardial action potential (AP) is an electrical phenomenon orchestrated by a variety of ion channels, exchangers and pumps that activate (open state) and inactivate/deactivate (closed state) in a highly regulated manner. Ionic currents are generated when ion channels open: allowing ions to flow down

their respective electrochemical gradient. The opening and closing of ion channels, and the currents they produce, generate the depolarization and subsequent repolarization of membrane voltage referred to as an action potential. Phases (0-4) of the action potential are highlighted in Figure 1.3.2 for a ventricular myocyte of larger mammals[34]. For a typical ventricular AP, there are five distinct phases (0-4) that describe the change in membrane voltage as a function of activating (and inactivating) time- and voltage-dependent ionic currents.

Phase 0

The initial depolarization is the result of voltage gated sodium channels opening that allow a substantial influx of Na^+ ions into the cell causing a change in membrane potential from roughly -70 mV to potentials as high as +40 mV. This dramatic change in voltage is referred to as phase 0 and in ventricular myocytes occurs on the order of milliseconds. The sodium current (I_{Na}) is governed primarily by Nav1.5 and is important in determining excitability and the upstroke velocity of phase 0. It has been shown by our lab that PKJ cells of the mouse have the highest upstroke velocity followed by ventricular myocytes and atrial myocytes. Nodal cells, specifically those of the SA and AV Node, have a relatively shallow upstroke velocity due the reduced presence of sodium channel isoforms (Nav1.1, Nav1.2 and Nav1.5). It has been shown that I_{Na} is reduced in these cells compared to other regions of the heart, but their contribution is a

necessity for normal SA node function[35]. Furthermore, there is considerable heterogeneity of I_{Na} density across nodal cells and this variability is further complicated by species dependent differences [36-39]. Nodal cells also rely on calcium currents (I_{Ca}) for phase 0, which have considerably slower activation kinetics. The first isoform of I_{Ca} found in pacemaker cells are those of T-type currents (I_{CaT}), which activate at relatively hyperpolarized potentials [40]. L-type calcium currents (I_{CaL}) are also expressed in both SA and AV nodal cells where they contribute to AP generation and regulating automaticity[36,41,42].

Phase 1

Following phase 0 there is a brief but rapid repolarization referred to as Phase 1. This repolarization has multiple underlying ionic factors. I_{Na}, responsible for phase 0, rapidly inactivates after passing current for only ~10 msec. Once the cell is depolarized (>$^{-}$30 mV), activation of voltage-gated potassium channels (Kv4.2/Kv4.3 and Kv1.4) cause a rapid hyperpolarization of membrane voltage. This outward shift in K^+ ions is relatively short in duration and is referred to as the "transient outward" potassium current (I_{TO}). Detailed kinetic analysis of I_{TO} in various species and regions of the heart suggests two types of I_{TO} currents underlie the total current[41]. Electrophysiological and pharmacological studies have provided considerable support for this hypothesis, including experiments detailed in subsequent chapters of this dissertation. In mouse ventricular myocytes, two transient potassium currents, termed I_{TOfast} and I_{TOslow} have been differentiated[43]. A major difference between the ventricular action potential of

mice and humans is that rodent I_{TO} is substantially larger in amplitude and is the predominant voltage-gated potassium repolarizing current. Therefore, rodents APs tends to be more triangular in shape and are considerably shorter in duration[44]. This is due to the rapid (~600 beats/min) heart rates in these animals[43,45]. In the canine heart, expression of I_{TO} varies between the epicardium, mid-myocardium and endocardium of the ventricular tissue; and this heterogeneity gives rise to the distinct shape of the ventricular action potential from each of these regions[44,46,47]. Similar differences in expression have also been shown in the mouse ventricular myocardium between the apex, septum and free wall[43]. Initial characterization studies suggested that I_{TOfast} and I_{TOslow} currents reflect two molecularly distinct Kv channels. I_{TOslow} channels inactivate more slowly than I_{TOfast} and recover from steady state inactivation on the order of seconds [43,48]. It was later shown that Kv1.4 underlies the I_{TOslow} component of I_{TO}. Another functionally important potassium channel is Kir6.2, which underlies the I_{KATP} current. These channels are predominately found in the ventricular myocardium and functionally alter Phase 1 of the myocyte APD [49]. This class of channel is inhibited by intracellular ATP, activated by nucleotide diphosphates and regulated by intracellular G proteins. It has been suggested that the regulation of this channel by ATP, functions as a metabolic link between myocyte metabolism and AP morphology [50 51]. This channel has been suggested to play a role during metabolic stress (e.g. ischemia or hypoxia) during which the channel opens and results in a shortened action potential duration[50,52,53].

Phase 2 and Phase 3

In larger mammals, Phase 2 of the action potential is characterized as a plateau due to the relative stability of V_m observed before final repolarization. The depolarization caused by the influx of sodium ions not only activates voltage gated potassium channels, but also activates voltage-gated calcium channels. In most cardiac cells, the L-type calcium channel (Cav1.2) is responsible for the inward and depolarizing current underlying phase 2[7,54]. I_{CaL} is ubiquitously expressed across cells in the myocardium [41,55]. In atrial and Purkinje cells of the conduction system, I_{CaT} (Cav3.1) contributes to phase 2, which is activated at more hyperpolarized potentials[30,55] and may prolong phase 2 in these cells[1,56]. The influx of calcium ions during phase 2 is the initial step in calcium-induced calcium release (CICR). CICR serves as the molecular trigger during excitation-contraction coupling [57 58], which is the translation of the electrical impulse into a contractile response. This phenomenon will be discussed in detail in subsequent sections.

In larger mammals, which do not have the characteristic triangular action potential of rodents, the action potential plateau is determined by a delicate balance between the inward calcium current (I_{CaL}) and the outward potassium currents (I_{Ks} & I_{Kr}) that flow primarily through the delayed rectifier voltage gated potassium channels (Kv7.1 & Kv11.1). The designations I_{Ks} (slow) and I_{Kr} (rapid) are based in differences in time- and voltage-dependent properties [59-61]. During late phase 2 and early phase 3, the delayed rectifier currents (I_{Ks} and I_{Kr}) progressively increase in a time dependent manner[62]. This increase in the

outward current, coupled with the inactivation of calcium currents, eventually leads to the termination of phase 2 and begins the final repolarization of the AP (phase 3). During phase 3, inward rectifier potassium channels (Kir2.x) “activate” and pass a hyperpolarizing current (I_{K1}). Hyperpolarization by I_{K1}, coupled with the inactivation of all other voltage-gated channels shifts membrane voltage to its resting state. I_{K1} plays a pivotal role in determining the steepness of phase 3 and in the overall resting potential(phase 4). As inward rectifiers, Kir2.x channel carry inward potassium currents with higher amplitudes than outward currents [63 64]. In physiological systems, membrane voltage does not reach E_K (~-90 mV) and therefore the outward component of these channels is far more important. I_{K1} channels have been characterized in most cardiac regions with reduced or no expression in SA and AV nodal cells, depending on the species[65,66]. I_{K1} is characterized by voltage-dependent block from magnesium, calcium and polyamines at potentials >-40 mV [67 68-71] and therefore is primarily engaged in the passage of current in the range of -40 mV to -90 mV.

Phase 4

In non-pacemaking cells, I_{K1} stabilizes the resting membrane potential, which in turn determines membrane excitability (Phase 4)[72]. A number of specialized cells of the heart, particularly SA, AV and PCs, demonstrate automaticity, a spontaneous phase 4 depolarization. Spontaneous phase 4 depolarization has been attributed to the presence of the funny current (I_f) [73]. The funny current flows through the hyperpolarization and cyclic nucleotide (HCN)

gated channels. I_f is a mixed Na^+/K^+ current, which activates slowly upon hyperpolarization and inactivates slowly in a voltage-independent manner upon depolarization. I_f conducts an inward current during phases 3 and 4 and has been suggested to be the primary current responsible for slow membrane depolarization in cells with pacemaker activity[74]. I_f activation is accelerated when intracellular cyclic adenosine monophosphase (cAMP) levels are increased. Furthermore, I_f modulates heart rate by sympathetic and parasympathetic activity[75]. Nodal cells also express I_{CaT}, which is activated at hyperpolarized potentials that contribute to spontaneous phase 4 depolarizations[40]. The sodium calcium exchanger (NCX) has been suggested to contribute an inward $I_{Na/Ca}$ component during phase 4 which may contribute to depolarization[76]. The mechanism by which the NCX directly contributes to phase 4 depolarization remains controversial and has been suggested to involve I_{CaT} triggering local calcium release from the SR[7].

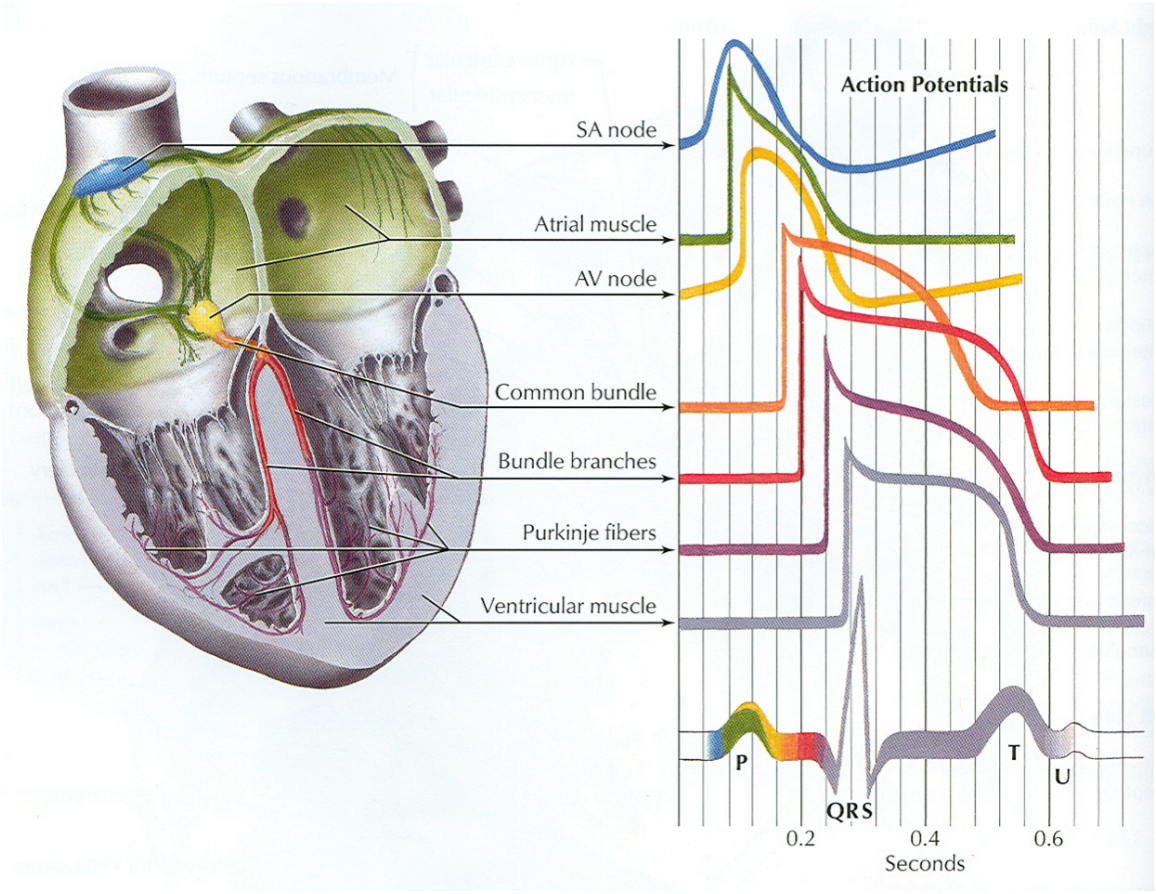

Figure 1.3.1: Mammalian heart demonstrating spatial and electrical heterogeneity in the cardiac action potential. Regions of the heart (left) are color coded and match with corresponding action potentials (right). Clinical measurement of the heart's electrical activity, via ECG, is shown (bottom right) with the various regions accounting for different peaks. Adopted from Nerbonne[4].

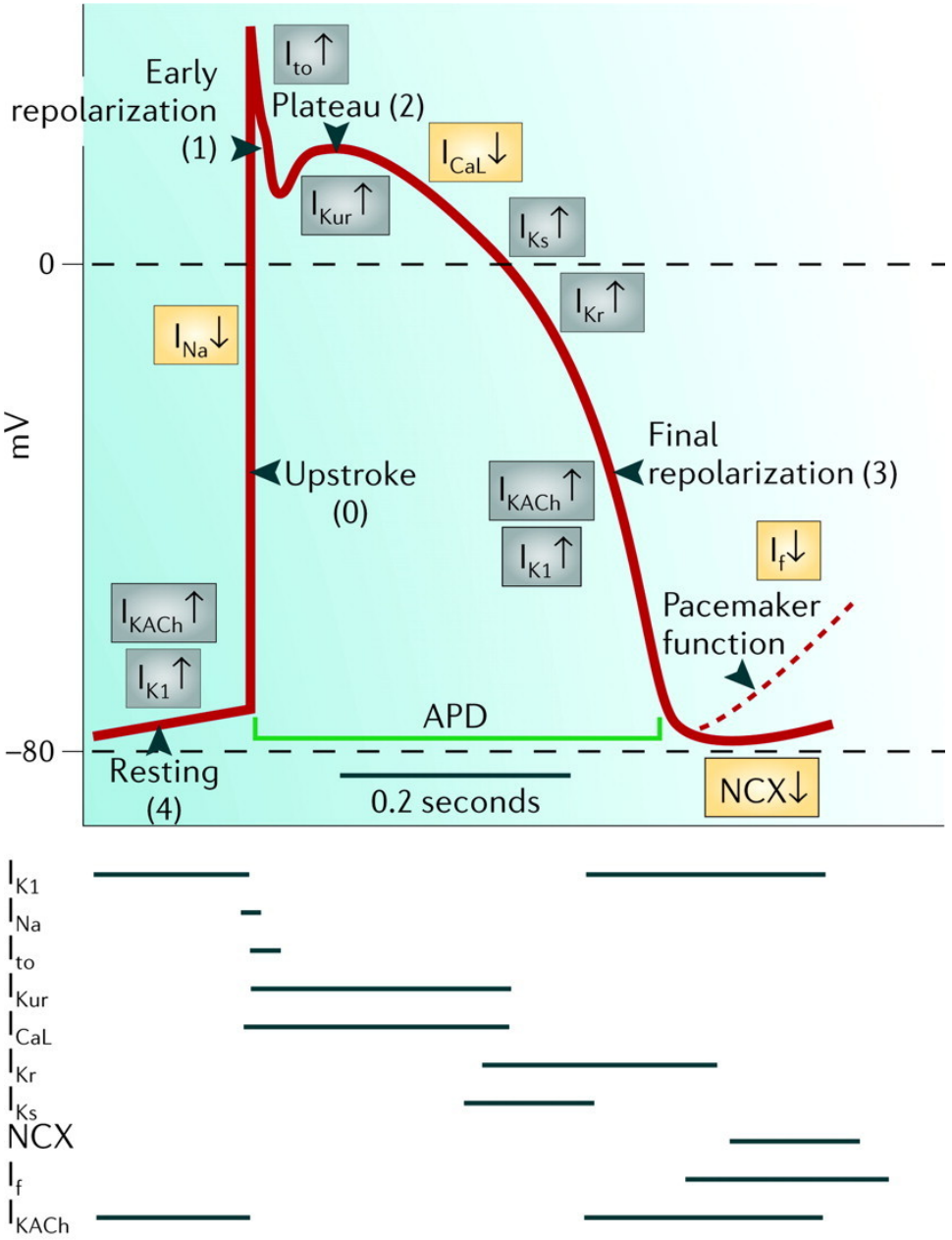

Figure 1.3.2: Membrane currents that generate the normal ventricular action potential. Resting (phase 4), upstroke (phase 0), early repolarization (phase 1), plateau (phase 2), and final repolarization (phase 3) are the 5 phases of the action potential. A decline of potential at the end of phase 3 in pacemaker cells, such as the sinus node, is shown as a broken line. The inward currents (INa, ICa and If) are shown in yellow boxes and the sodium calcium exchanger (NCX) is also shown in yellow although it may generate inward or outward current. IKAch, IK1, ITO, IKur, IKr and IKs are shown in gray boxes. [6]

1.4 Excitation-Contraction Coupling

Introduction

Excitation-contraction (EC) coupling is the translation of the cardiac electrical impulse into a contractile response. The regulation and synchronization of this process is critical for normal cardiac function. The influx of Ca^{2+} ions during an action potential are essential as a second messenger in EC coupling and is the direct activator of the myofilaments[77]. Disruption of calcium homeostasis is a central cause of both contractile dysfunction and arrhythmias[78].

Major Structures Involved in Excitation-Contraction Coupling

1.4.1 Lateral Sarcolemma

The sarcolemma is the primary location of two calcium pumps involved in maintaining calcium homeostasis: the Ca-ATPase pump and the Na/Ca exchanger (NCX). The Ca-ATPase pump is ubiquitous in all cells (Schatzmann, 1982, 1989; Carafoli & Stauffer, 1993; Guerini 1998) and was first discovered in erythrocytes. Two key features of the Ca-ATPase are its stimulation by Ca-calmodulin and by PKA-dependent phosphorylation. However, experimental data suggest the sarcolemmal Ca-ATPase contributes only a small fraction of overall calcium removal from the cytosol (~1%) whereas the NCX (~30%) and sarcoplasmic reticulum bound Ca-ATPase (SERCA, ~70%) account for the majority of calcium extrusion from the cytoplasm during diastole (reviewed in Bers et al, 2002[7]).

1.4.2 Transverse Tubule Network

Transverse tubules (t-tubules) of cardiac myocytes are invaginations of the sarcolemma that create a tubular network through the myocyte core. T-tubules play a pivotal role in excitation-contraction (EC) coupling by allowing the action potential (depolarized membrane) to propagate into the cell interior. Furthermore, t-tubules contain a variety of calcium-handling proteins involved in the initiation and termination of contraction and provide proximity between the excitable cell membrane and the sarcoplasmic reticulum[7]. Originally, t-tubule structures were defined as lateral (transverse) structures present solely at the Z-line, with a regular sarcomeric interval of ~2 μm[79]. Interestingly, subsequent studies revealed the t-tubule network to be significantly more complex than originally suggested[3]. Figure 1.4.1 demonstrates the longitudinal extensions connecting the transverse sections at the Z-line. The widespread longitudinal extensions account for roughly 40% of the tubular volume with the transverse tubular system near the Z-line accounting for the remaining ~60%. A number of studies have called for renaming the “transverse tubule” system due to the accepted complexity beyond a transverse architecture[3,77,80]. However, “t-tubules” remain the standard terminology encompassing the entire sub-sarcolemma tubular network of cardiac myocytes. Functionally, t-tubules are responsible for the rapid propagation of the electrical impulse deep within the core of myocytes, which allows for calcium entry to occur near all sarcomeres uniformly regardless of how deep they lie within the cell.

Estimates of the cell volume occupied by t-tubules ranges from 0.8% to 3.6% in rat and mouse ventricular myocytes, respectively[3,81]. The percentage of ventricular cell membrane located within the t-tubule network varies from ~15% to >50% with no apparent species dependent differences[3,82-84]. Individual t-tubules have a diameter ranging from ~20 – 450 nm with a significant majority closer to the mean diameter of ~230 nm in the rat[3]. T-tubules are present in the cardiac tissue of all species of mammals thus far investigated[3,85-89]. However, t-tubules appear to be absent in amphibian, avian and reptile cardiac myocytes[81,90].

The molecular mechanisms governing t-tubule development and maintenance remain unclear. A number of observational studies demonstrated t-tubules form after birth when ventricular pressures rise[86] and are absent from isolated neonatal ventricular myocytes[91]. At present, a number of studies have suggested the development and maintenance of t-tubules are regulated by biochemical (e.g. amphiphysin 2, myotubularin, etc.) and biophysical factors (e.g. load, heart rate, etc.) [88,92,93]. *In vitro* analysis of t-tubule formation and maintenance is complicated by the deterioration of t-tubule structures during cell culturing, which may be due to the lack of biochemical and biophysical regulators found in the intact myocardium[94]. Information regarding the structural components of t-tubules comes primarily from immunocytochemistry experiments. Such studies have shown marked variations in the distribution of t-tubule membrane proteins. Primarily, t-tubules contain calcium-handling proteins involved in EC coupling which will be described in subsequent sections. Recently, a small number of proteins have been described to play important biogenesis

and maintenance roles of t-tubules. Junctophilin proteins are members of a family of junctional membrane complex-associated proteins found in all excitable cells[95]. Junctophilin-2, the major cardiac isoform, has been shown to be involved in tethering the SR to the t-tubules by spanning across both membranes. Inducible knockdown models of Junctophilin-2 have demonstrated its critical role in t-tubule maintenance and synchronous calcium release from ryanodine channels on the SR[95-98]. Telethonin or Tcap, is a 19 kDa protein primarily found at the Z-disc. Similar to Junctophilin-2, knockdown studies in mice have demonstrated a loss of Tcap remodels the t-tubule structure and function[99]. These proteins may be important markers and potential therapeutic targets during t-tubule remodeling.

1.4.3 Calcium Channels

The role of calcium as a critical component of contraction of the myocardium has been known since the time of Ringer over 130 years ago [100]. Calcium channels were first characterized a “slow inward current” as it took 10s of msec for the peak current to be achieved compared to the fast activation of sodium currents [101]. In cardiac myocytes, the slow inward current prolongs the depolarization of the action potential and contributes to the plateau of the action potential (phase 2).

Calcium Channel Isoforms and Expression

The primary goal of the electrical impulse that propagates across the myocardium is to elicit a mechanical response. This phenomenon is known as excitation-contraction coupling (EC coupling) and will be discussed in subsequent chapters of this introduction. The first step in EC coupling, which will be discussed in depth here, involves the influx of calcium ions from the extracellular space through calcium selective ion channels. Bean et al [55] was the first to demonstrate two distinct classes of calcium channels in the heart. The two classes of calcium channels are present in cardiac tissue are the L-type (low threshold type), which is ubiquitously expressed in all cardiac cell types by the *CACNA1C* gene. The alternate isoform of calcium channels in the heart are encoded by the *CACNA1G* gene are its expression of the T-type (transient type) channel is localized to the conduction system and atrial myocytes[55,102].

Structure and Localization of Calcium Channels

A total of five protein subunits (α1c, α2, β, γ and δ) have been found to constitute the Ca^{2+} channel *in vivo*[103-106]. The α1c subunit comprises the main functional characteristics of Ca^{2+} channels: pore forming domain, DHP, phenylalkylamine and benzothiazepine receptors [107-112] and contains sites for phosphorylation by protein kinase A, CAMKII and protein kinase C[113-116]. Functional α1 channels consist of four homologous domains, I-IV, each consisting of six transmembrane spanning segments and a loop between segments 5 and 6 that dips back into the membrane and is responsible for forming the selectivity pore (P loop). Like other voltage gated ion channels, the

S4 domain has repeating positively charged amino acids at every third residue responsible for voltage sensitivity. The α1 subunit has classically been defined by its sensitivity to dihydrophyridines. Many act as Ca^{2+} antagonists (e.g. nifedipine, nisoldipine and nitrendipine). However, other DHPs act as agonists of LTCC function (e.g. Bay K 8644). The heart contains both α1c and α1d channels (also an L-type channel), but there is currently no clear functional consequence to α1c and α1d expression [117].

In vivo, calcium channel α subunits are typically associated with a variety of auxiliary subunits. The α2 & δ subunit are spliced from the same α2δ gene and cleaved resulting in two different protein products[106]. When the α2/δ proteins are coexpressed with α1c there is a ~2 fold increase in expression of the DHPR binding sites, gating currents and ionic currents[118,119]. These observations indicate that α2 and δ proteins play a role in the formation of functional channels at the plasma membrane. The structure of the δ component is membrane spanning and has been postulated as an anchor for the entire α2δ complex. It consists of a short cytosolic COOH terminus, a single transmembrane segment and a short extracellular domain, which is linked via a disulfide bridge to the heavily glycosylated and much larger (~200 kD) α2 subunit. The intracellular COOH terminus of δ is 1-15 residues long and is unlikely to be phosphorylated by protein kinases(83). The heavily glycosylated and entirely extracellular α2 subunit has been shown to interact with the α1 subunit in domain II[120]. Eight genes encode γ subunit of Ca_v channels. Recently, it was determined that γ4, γ6, γ7 and γ8 physically interact with the cardiac Cav1.2 complex in the presence or

absence of the α2/δ subunits[121]. Modulation of I_{CaL} by γ subunits was reported to be isoform specific, dependent on the subtype of β subunit present and the presence or absence of the α2/δ subunit. The role of γ subunits on Cav1.2 localization has not been investigated.

Currently, there are four Cavβ subunit genes (*CACNB1-4*) with the main cardiac isoform being the Cavβ2[122,123]. Each Cavβ2 subunit has three variable regions flanking two highly conserved domains(89, 222,[123]. The variable regions are in the COOH termini, the NH2 termini and a small (roughly 100 a.a.) region in the center of the linear protein sequence between the two conserved domians [122-124] [124,125]. The conserved domains mediate Cavβ2 interactions with the pore forming α subunit. The variable domains influence the function effects of Cavβ2 coexpression on the properties of the resulting Cav1.2 channels [126]. It has been suggested that Cavβ2 subunit binds to the cytoplasmic loop that links repeats I and II of the α1 subunit[127]. A highly conserved 30 amino acid motif within the β subunit is required for its interaction with the α1 subunit [127]. Coexpression of β2 with α1c causes a 10-fold increase in current, accelerates activation and inactivation kinetics, shifts steady-state inactivation and greatly increases the number of high affinity DHP binding sites [123,128] [129]. It is believed that the β subunit may act as a molecular chaperone, helping nascent α1c peptides fold properly and reach the plasma membrane by masking an endoplasmic reticulum signal on the cytoplasmic I-II loop of the α subunit [130] [131].

Localization of Cav1.2 to t-tubule microdomains is essential for normal cardiac function. Recently, it was suggested that BIN1 (amphiphysin 2) is criticial

for Cav1.2 trafficking and anchoring in the t-tubule milieu[92]. There is considerable evidence suggesting trafficking of Cav1.2 to the t-tubules occurs via microtubules[132-134]. BIN1 was also shown to play an important role in the forward trafficking mechanism of Cav1.2 and that BIN1 anchors microtubules, which may aid in offloading of Cav1.2 containing vesicles to the t-tubule membrane[92]. BIN1 is a member of the BAR domain containing protein family, which has a role in membrane bilayer deformation at endocytic sites through interactions between their N-terminal positively charged BAR domains and acidic phospholipids within the cell membrane[135]. It has been shown previously that BIN1 can induce enormous membrane invaginations in both non-t-tubule forming atrial HL-1 cells and non-cardiac HELA cells [92,136]. Mislocalizaton of Cav1.2 to the t-tubule membrane has detrimental effects on EC coupling and calcium handling. These effects will be covered in depth in the "Cardiac Remodeling" section.

Functions of Calcium Channel Isoforms

Cav1.2 is the pore forming subunit of the L-type Ca^{2+} channels (LTCCs), which are characterized by a large conductance (~25 pS in 110 mM Ba^{2+}), long lasting openings (in Ba^{2+}), sensitivity to 1,4 dihydropyridines and activation at larger depolarizations (i.e. more positive E_m). Maximal activation is primarily occurs at ~0 mV in mice and is right shifted (+20 mV) in sheep and larger mammals. These voltages roughly correspond with phase 2 of the action potential. Therefore, the positive inward current, along with the inactivation of outward (repolarizing) potassium currents, is responsible for the action potential

plateau. LTCCs are primarily responsible for the influx of extracellular calcium, which triggers the opening of ryanodine channels on the sarcoplasmic reticulum causing a dramatic rise in intracellular Ca^{2+} concentration $[Ca^{2+}]_i$. This dramatic spike in $[Ca^{2+}]_i$, via the ryanodine receptors, is critical for muscle contraction.

The alternate isoform of calcium channels found in the heart are T-type Ca^{2+} channels (TTCCs). TTCCs are localized to pacemaker, atrial and PKJ cells of the conducting system. Unlike L-Type channels, TTCCs are characterized by a tiny conductance (~8 pS in 110 mM Ba^{2+}), transient openings, insensitivity to DHPs and activation at a more hyperpolarized E_m. Activation at hyperpolarized potentials, the distribution to pacemaker, atrial and PKJ cells has led to the hypothesis and supportive evidence for the role of TTCC current (I_{CaT}) in pacemaker activity [30]. Interestingly, cardiac cell types where I_{CaT} is present also happen to be cells that lack extensive T tubules. However, this relationship is not always the case. I_{CaT} may be present in developing ventricular myocytes and during ventricular hypertrophy in the rat[137,138].

1.4.4 Sarcoplasmic Reticulum and Ryanodine Channels

The sarcoplasmic reticulum (SR) is an intracellular, membrane bound compartment found in myocytes. The SR's primary role is release and sequestration of Ca^{2+} ions to and from the cytoplasm, which are responsible for contraction and relaxation of cardiac muscle. Due to the SR's pivotal role in translating the electrical impulse into a contractile response, the architecture of the SR is highly specialized into two major regions:

(1) The junctional SR are the junctions of the SR that come in direct contact with the sarcolemmal invaginations which from the t-tubules. The junctions are referred to as “dyads” due to coupling of a single junctional SR domain with a single t-tubule domain. This arrangement is characteristic of vertebrate cardiac myocytes. An alternative arrangement that is noted in skeletal muscle, in which a single t-tubule is paired with two junctional SR domains, is referred to as a “triad”. The close relationship of the L-type calcium channels (LTCCs) of the t-tubules with ryanodine channels in the junctional SR is primarily responsible for the release of calcium from the SR during systole. This site is effectively the initiation point of EC coupling.

(2) The SR network runs along the length of the sarcomere and contains densely packed calcium pump ATPase proteins (SERCA) responsible for the reuptake of calcium during diastole.

Ryanodine receptors (RyR2) are SR membrane bound channels at the subsarcolemmal cisternae that form junctions with the LTCC and t-tubule membrane. RyR2 also localize a number of regulatory proteins to the junctional complex. These include calmodulin, FK-506 binding protein and PKA among numerous others involved in Ca^{2+} buffering and modulation of the Ca^{2+} release process. Calmodulin exerts Ca^{2+} dependent modulation of RyR2 function[139]. FK-506 binding protein has been suggested to stabilize RyR gating[140]. PKA plays an important role during β adrenergic stimulation and alters the gating of RyR2 and the LTCC. RyR2 proteins are arranged in large organized arrays at the cisternae

junctions with diameters up to 200 nm containing ~100 RyR2 proteins [96]. These arrays constitute a large functional Ca^{2+} release complex at the junction known as a couplon[141]. Couplons are the molecular correlate of experimentally observed "Ca^{2+} sparks" that reflect nearly synchronous activation of a cluster of about 6-20 RyR2's at a single junction, which is central to the model of EC coupling [142-144].

1.4.5 Electro-Mechanical Transduction

In the myocardium, Ca^{2+} ions are fundamental in translating the electrical stimulus (action potentials) into a mechanical response (contraction). The cyclical release and sequestration of Ca^{2+} ions is maintained by multiple types of membrane and organelle bound Ca^{2+} channels and transporters. Their orchestral-like involvement in excitation, contraction and subsequent relaxation of the myocardium during the cardiac cycle is referred to as calcium homeostasis. At the onset of a depolarization, L-type Ca^{2+} channels (LTCCs) shift their orientation and open, allowing Ca^{2+} ions to permeate into the cytoplasm (I_{CaL}). The LTCCs are chiefly localized at the t-tubular membrane of the cardiac myocyte[145]. In ventricular cells, this localization allows for the propagation of the electrical impulse to drive uniform increases in cytosolic Ca^{2+} concentration via t-tubule entry versus diffusion of Ca^{2+} ions solely from the sarcolemma. The localization of LTCCs is complemented by the SR's previously mentioned subsarcolemmal cisternae. This positioning allows close proximity to ryanodine receptor (RyR2) channels located at the junctional membrane of the sarcoplasmic reticulum (Figure 1.4.2). Ca^{2+} ions that flow through LTCCs bind to

RyR2 channels triggering a substantial release of Ca^{2+} ions, through opened RyR2 channels, from the sarcoplasmic reticulum into the cytosol resulting in an increase of intracellular calcium $[Ca^{2+}]_i$ from ~100 nM to ~1 μM[146]. The influx of Ca^{2+} ions through LTCCs and the triggered opening of ryanodine receptors is termed Calcium Induced Calcium Release (CICR). As Ca^{2+} ions permeate throughout the cell, they bind to troponin C on the actin filament which changes the configuration of tropomyosin allowing the actin-myosin interaction and filament sliding due to the movement of the myosin head after actin binding[7]. In order for relaxation to occur, ATP dependent transporters must restore the intracellular calcium concentration to resting levels by re-sequestering Ca^{2+} ions into the sarcroplasmic reticulum (SERCA2a) and pumping Ca^{2+} out of the cell (NCX). The sequential cellular increase and SR sequestering of Ca^{2+} ions in the cardiac cycle is paramount in maintaining intracellular calcium homeostasis. Therefore, tight regulation of intracellular Ca^{2+} ion flux is critical for proper physiological function of the myocardium. Altered states of Ca^{2+} homeostasis have been implicated in a multitude of cardiac diseases ranging from arrhythmias to cardiomyopathies[147-150].

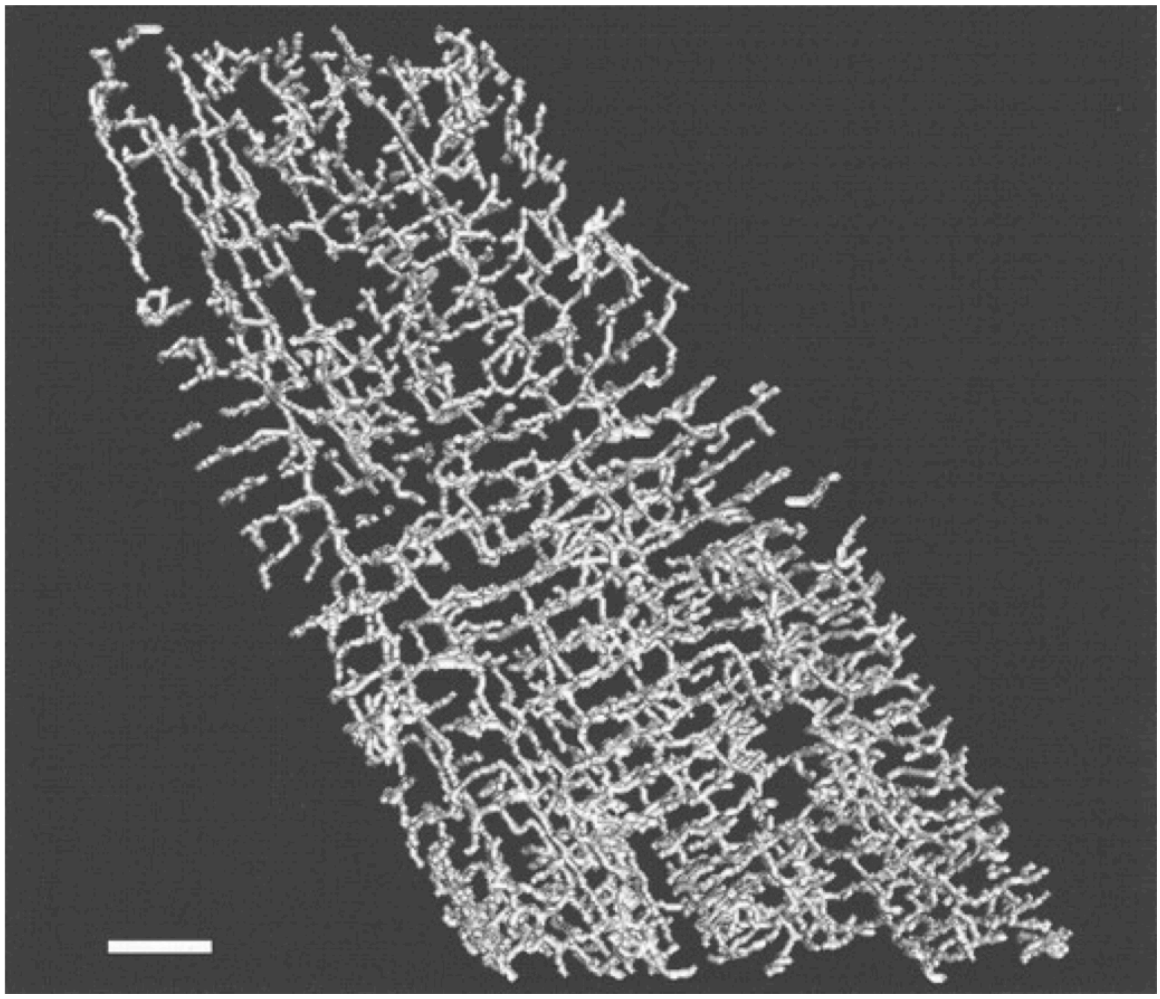

Figure 1.4.1: Three-dimensional skeleton of the t-tubular system in a rat ventricular myocyte. The skeleton was reconstructed from a deconvolved stack of images (an example of which is shown in Figure 3). The overall macroarchitecture resembles a complicated 3D mesh with some imposed regularity. Note that in some regions of the cell many tubules run axially and in other directions rather than transversely. Scale bar=5 μm.[3].

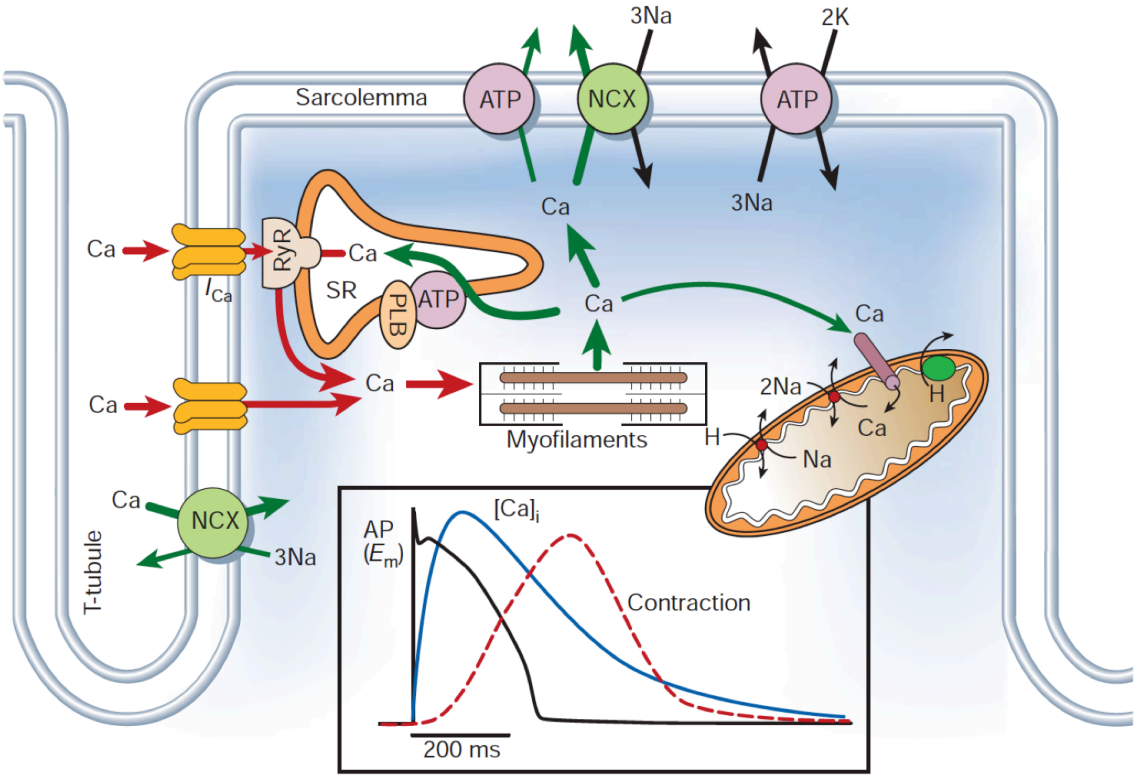

Figure 1.4.2: Schematic representation of calcium handling in a traditional ventricular myocyte. Inset shows the time course of an action potential, Ca^{2+} transient and contraction measured in a rabbit ventricular myocyte at 37°C. Calcium ions flow in the direction of the arrows (red: entering cytoplasm; green: leaving cytoplasm). Initially, Ca^{2+} ions enter the cell through LTCCs and directly activate RyR2 channels, which in turn empties the SR's calcium reservoir. Increases in cytosolic calcium allow causes Ca^{2+} ions to bind to the myofilaments, initiating contraction. Calcium is extruded from the cytosol via ATP driven transports on the SR (SERCA) and sarcolemma membrane (NCX & Ca-ATPase)[7].

1.5 Cardiac Remodeling During Disease

1.5.1 Introduction

Traditionally, cardiac remodeling is defined as an alternation in the structure of the heart (dimensions, mass, shape) in response to hemodynamic load and/or cardiac injury in association with hormonal activation. This definition, through advancements in basic and clinical observations, has come to encompass alternations and changes related to electrical activity of the myocardium as well as structural abnormalities. Furthermore, remodeling may be described as physiologic or pathophysiologic [151]; alternatively, remodeling may be classified as adaptive or maladaptive[152] and is described in detail below:

- Physiological remodeling is a compensatory change in the dimensions and function of the heart in response to physiologic stimuli such as exercise and pregnancy.

- Pathophysiological remodeling may occur with pressure overload (e.g. aortic stenosis, hypertension), volume overload (e.g. valvular regurgitation), or following cardiac injury (e.g. myocardial infarction, myocarditis, or idiopathic dilated cardiomyopathy). In each of these diseases, remodeling may transition from an apparently compensatory process to a maladaptive one [153].

This section will focus on pathophysiological remodeling in context of atrial fibrillation (electrical) and heart failure (structural).

1.5.2 Electrical Remodeling: Atrial Fibrillation

Atrial fibrillation (AF) is the most common cardiac arrhythmia in adults and affects 2 to 5 million Americans per year[154]. AF is the number one cause of hospitalization for arrhythmias and its incidence is predicted to double in the next two decades[155-158]. AF is associated with a wide range of potential complications and contributes significantly to population morbidity and mortality. Yet, the therapeutic management for AF is highly complex and a large percentage of patients still await novel therapies. In the last decade, the emergence of catheter ablation for AF has highlighted the role of the posterior left atrium (PLA)-pulmonary veins region in the initiation and maintenance of the arrhythmia[159]. However, the mechanisms of AF perpetuation involving the PLA are incompletely understood but considered to be a site important in atrial remodeling.

The concept of atrial electrical remodeling was introduced as early as 1995 by Wijffels et al[160] who demonstrated that AF in goats induces functional alternations that favor the maintenance of AF. This seminal work came to characterize the electrical remodeling in AF as a phenomenon in which “AF begets AF”. Their characterization of atrial remodeling during AF encompassed the idea that altered atrial structure or function increases the likelihood of ectopic and reentrant (fibrillatory) activity[161]. This is coupled in part, by the changes in the electrophysiological patterns of atrial tissue, which favor rapid pacing (tachycardia) versus normal sinus rhythm. Atrial tachycardia and the predisposition to reentrant or ectopic activity, are supported by regional

heterogeneity of action potential duration (APD) and by abnormalities in atrial conduction properties[160,162-164]. In addition, there is evidence of enhanced focal atrial driver activity[164], possibly related to triggered activity associated with calcium handling abnormalities [165 166].

Ion channel remodeling

Understanding ion channel remodeling is a key dynamic in generating improved treatment and management of AF. Voltage-clamp experiments conducted in a canine tachypaced model reduces current density of I_{Na}, which was paralleled by, decreases in mRNA expression and conduction velocity[167]. However, in a study of ionic remodeling in AF patients, no reduction in I_{Na} was observed [168]. Similar observations were seen in a goat model of AF. These conflicting reports suggest I_{Na}, Nav1.5 protein content and Nav1.5 mRNA dependent remodeling are species specific. Unlike I_{Na}, changes to inward rectifier (I_{K1}) currents appear less complicated. Several studies have reported increased background I_{K1}, in atrial myocytes from AF patients [168 169-173]. These observations have been supported in canine studies[174,175]. I_{K1} increases correspond to more negative resting membrane potentials in both models. Increased Kir2.1 mRNA and protein expression has also been observed in AF patients [169,171]. Atrial tachycardia models demonstrate consistent downregulation of voltage-gated potassium currents (I_{TO}). Reductions were observed as early as 24 hrs and progressive downregulation was observed over 6 weeks in animal models and patients with AF [167,168,172,173,176]. However, the functional significance of I_{TO}

changes are not clear. Decreased I_{TO} has relatively minor effects on human and canine atrial APD[177,178]. Reports on other voltage-gated potassium currents (IKur) have been conflicting[167,172,173]. However, I_{Kur} remodeling during AF continues to be an appealing target for anti-arrhythmic therapy as it is an atrial specific current. At present, there are no observed remodeling of I_{Ks} or I_{Kr} currents in animal models or human AF patients[167].

Atrial tachycardia results in significant alterations in calcium handling. Increases in calcium load[179], due to rapid pacing, result in reductions of I_{CaL}. These reductions have been consistent in a number of animal models and AF patients [167,168,173,180]. Consistent with changes in I_{CaL}, mRNA for the α subunit of Cav1.2 has shown similar reductions[168,181,182] and studies quantifying Cav1.2 protein have also shown reductions in total protein content[182-184]. However, I_{CaT} does not appear to be affected in a similar fashion to I_{CaL}[167]. Pharmacological block of I_{CaL} reproduces the electrophysiological remodeling observed during AF e.g. APD abbreviation [167,168,180]. Consistent with reductions in I_{CaL}, AF models demonstrate reduced calcium transients and a slowed decay[179]. Furthermore, these alterations in calcium handling cause myocyte contractile dysfunction [179]. These observations have supported by similar data in AF patients[185]. It has been suggested that during the remodeling process, hyperphosphorylation of the RyR2 receptor and causes increased activity of the RyR2 channel. Therefore, patients with AF demonstrate more frequent calcium sparks and calcium waves [186]. At present, there are conflicting reports regarding the activity, mRNA content and protein levels of SERCA2a, NCX, calsequestrin and phospholamban which are

all crucial components of calcium handling and extrusion from the cytoplasm [184,185,187-189]. It has been suggested these differences may be attributed to the high variability in age, sex, co-morbidities, drug treatment and stage of AF for each patient.

At present, the mechanisms underlying ion channel remodeling in AF remain to a large extent, unknown. CaMKII upregulation in AF may underlie changes in I_{TO} [190] and the aforementioned hyper-phosphorylation of RyR2 channels promotes sarcoplasmic reticulum calcium leak[165]. Post-translational modifications (e.g. nitrosylation, dephosphorylation) have been suggested to alter ICaL[191,192]. The complexity surrounding atrial remodeling during AF is further complicated by hormonal regulation (e.g. angiotensin II, TGFβ, PDGF etc.), from the increased presence of fibrosis, a form of structural remodeling. These biofactors are currently an active area of research and may provide insights to the signal transduction pathways associated with ion channel remodeling.

1.5.3 Structural Remodeling: Heart Failure

Heart failure (HF) is often described, as an inability of the heart to meet hemodynamic needs of the body. Typically, HF is the result of multiple cardiac diseases and the prevalence and incidence of HF are rising [193]. Due to the severity of remodeling that takes place during the progression of HF, the 5-year survival rate is as low as 25% in men and 38% in women [194]. The development of HF is associated with progressive changes in ventricular chamber geometry and myocardial architecture, which are directly associated with continuous

reorganization of the cardiac extracellular matrix [195]. This structural remodeling impacts mechanical performance of the heart in multiple ways and similar to the remodeling associated with AF, causes a positive feedback mechanism in the remodeling process. Furthermore, the initial remodeling phases are compensatory and as the disease and remodeling progresses, eventually become maladaptive. As an example, hypertensive heart disease results in concentric left ventricular hypertrophy and increased collagen expression (pro-fibrotic) and initially these responses compensate for increased pressure load. Left ventricular end-diastolic volume remains normal and ejection fraction is preserved[196]. Eventually, the compensatory mechanisms lead to impaired diastolic function. End-diastolic volume becomes compromised at higher heart rates and as a result, stroke volume falls. Myocardial infarction has been shown to be associated with different mechanisms of compensation but the progressive maladaptation and tissue remodeling. However, both these diseases manifest a common phenotype in the final phases of HF. This section will focus on the progression of HF from the perspective of hypertensive heart disease.

A variety of animal models have been used to study the remodeling that occurs due to hypertensive heart disease and its progression to HF with the majority consisting of aortic banding [196] or genetic models [197]. At the onset, cardiac remodeling in response to hypertension is associated with increased myocyte cross-sectional area as the result of increased sarcomeres[196]. This leads to a preservation of ejection fraction coupled with impaired diastolic function due to left ventricular stiffness associated with increased fibrosis[198]. This

compensation results in the inability to increase cardiac output during elevated heart rates (e.g. exercise) and pulmonary venous pressures elevate [198]. Experimental observations demonstrate a transition to HF once the hypertensive heart develops a dilated left ventricle and a marked reduction in ejection fraction. During this progression, a number of pro-fibrotic factors are elevated due to the structural rearrangement of the ECM. Collagen synthesis increases due to the activation of TGFβ signaling pathways and reduced collagen degradation. Increased deposits of type I collagen and cross-linking results in severe interstitial fibrosis [199]. Continuing proliferation of interstitial fibrosis is directly responsible for progressive left ventricular dilatation and wall thinning. Currently, the role of collagen in the transition from a hypertensive heart to a dilated failing heart, whether there is increased deposition or decreased breakdown of collagen during this transition, remains controversial[199-201].

Cardiac myocyte structure and calcium handling are also adversely affected by HF remodeling. He et al first identified a significant loss of t-tubule density (without t-tubule disorganization) in ventricular myocytes from a dog model with pacing-induced HF [85]. Subsequently, a number of other studies using other animal HF models have reported profound t-tubule remodeling, including both loss and/or disorganization in ventricular myocytes [202 203,204]. These findings are consistent with human studies of HF showing pronounced loss of t-tubules in all forms of HF (ischemic heart disease, idiopathic dilated cardiomyopathy and hypertrophic obstructive cardiomyopathy)[205]. T-tubule loss and/or disorganization has been directly linked to dyssynchronous calcium sparks, reduced and slowed

calcium transients [202] [203,204]. In these studies, the demonstration of t-tubule loss was present at late stage HF. Recently Wei et al showed t-tubule loss occurring in the early stages of hypertension (Figure 1.5.2) They theorized progressive deterioration of t-tubule structure during hypertension and the strong correlation between t-tubule remodeling and left ventricular function support the notion that t-tubule remodeling is a critical factor during the transition from compensated hypertrophy to HF[2].

1.5.4 Metabolic disease associated with cardiac remodeling

Obese and overweight individuals are traditionally defined by a body mass index (BMI) with a scale ranging from: underweight being <20 kg/m^2, normal weight 20-25 kg/m^2, overweight 25-30 kg/m^2; class I obesity 30-35 kg/m^2; class II obesity 35-40 kg/m^2 and class III obesity >40 kg/m^2. Over the last twenty years, there has been a particularly striking increase in North America of men and women who fall in each of the three classes of obesity [206,207]. Obesity is strongly associated with the development of major risk factors for atherosclerotic disease such as hypertension, hyperlipidemia, and diabetes [208-210]. In addition, mounting evidence suggests that obesity also has direct effects on the heart that are not the result of comorbidities. Furthermore, obesity has been shown to have profound structural and functional alterations to cardiac tissue in both humans and animal models. A number of studies have suggested that long-term obesity will eventually lead to heart failure [211-213]. This association was further supported by the seminal work of The Framingham Heart Study, which demonstrated that

increased BMI was associated with an increased risk of heart failure in both men and women and that this risk was graded across categories of BMI (Figure 1.5.3)[214]. However, the direct link between obesity and associated cardiac remodeling remains unclear.

A variety of animal models (mice, rat and rabbit) have been used to investigate the underlying mechanisms that contribute to cardiac remodeling and dysfunction in obesity. To date, the majority of studies have focused on mouse models due to the ease in generating transgenic lines with targeted mutations in cardiac myocytes. Furthermore, a number of mouse models have been developed using diet-induced obesity, which is achieved by feeding animals a "high-fat" diet. The well-known *ob/ob* mice are null for the leptin gene and develop hyperinsulinemia and impaired glucose tolerance between 10 and 15 weeks of age[215]. The major drawback to genetically modified animals like the *ob/ob* mouse are the drawbacks in evaluating cardiac phenotypes e.g. age at which the studies are performed, potentially confounding effects of hyperglycemia and most importantly, determining which cardiac alterations are a consequence of obesity versus the loss of leptin-mediated signaling which is present in human obesity. Many recent transgenic lines have been developed to introduce mutations that increase free fatty acid (FA) uptake to levels that exceed the metabolic capacity of the mitochondria. Overexpression of peroxisome proliferator-activated receptor (PPAR)-α induced lipotoxic cardiomyopathy that was worsened on diets that were high in saturated long-chain. This study also found these PPAR-α mice had improved cardiac phenotypes when fed medium-

chain FAs[216,217]. Interestingly, another group generated PPAR-δ knockout mice in, which limits FA metabolism[218]. These mice are characterized by significant lipid accumulation in the absence of increased lipid uptake pathways and metabolism (PPAR-α mice) of FAs and develop heart failure[219]. Diet-induced obesity, achieved by feeding animals high-caloric chow, have suggested that diets with increased saturated fat content, or exposure of cultured cells to saturated FA promote cardiac dysfunction[220 221-223].

In humans and animal models, there is evidence for structural remodeling associated with obesity. Many published studies on human patients have suggested that obesity is independently associated with left ventricular hypertrophy (wall thickness and cavity size) through noninvasive imaging e.g. echocardiography, MRI etc. with only one study showing no association[224-229]. To date, there is little information regarding the biochemical and ultrastructure composition of cardiac myocytes in obese humans compared to HF animal models. Increased cardiac mass (particularly the left ventricle) has been associated with increased epicardial fat depots and increased fatty infiltration of the myocardium [230-232]. Using MRI spectroscopy, Iacobellis et al[231], quantified the triglyceride content in human myocardium and found it to be significantly increased in obese compared to normal-weight individuals. Peterson et al[233] further supports these findings by demonstrating obese subjects have increased myocardial fatty acid uptake and utilization. However, the direct effects of increased cardiac adiposity, infiltration, uptake and utilization remain unclear.

1.5.5 Epicardial Adiposity As a Source of Metabolic Biofactors

There is increasing evidence that excess epicardial adiposity is also arrhythmogenic[234-237]. Abnormal rhythms in the atrial and ventricular chambers have been associated with increases in adiposity, akin to those observed in obese patients, aging and certain pathological conditions affecting the heart[238]. Recently, independent reports have demonstrated a direct relationship between obesity and AF risk, incidence and/or persistence[237,239-243]. In humans, it has been shown in multivariable models adjusted for cardiovascular risk factors that there is a 4% increase in AF risk per 1-unit increase in BMI in both men and women[244-247]. However, the underlying mechanisms for the association between obesity and AF remodeling are largely unknown. This association may be linked to the increase in mass and infiltration of epicardial adipose tissue into the myocardium[248]. The increase in epicardial adipose tissue also elevates the secretion of adipocyte biofactors, which exert paracrine effects on the localized myocardium and has been shown to remodel myocyte electrophysiology[237,249]. Adipocyte biofactors are generally classified under metabolic modulators, cytokines, vasoactive regulators and growth factors[250,251]. There is evidence that of these categories, FAs released by adipocytes may also modulate heart muscle function. The electrophysiological effects of polyunsaturated free fatty acids (PUFFAs), e.g. arachidonic and docosahexanoic acids on cardiac myocytes are generally recognized and may have antiarrhythmic benefits[252-255]. However, similar to obese mouse models, it has been suggested that long chain saturated FAs may alter atrial myocyte electrophysiology[256]. To date, there are no large

mammal studies investigating how saturated FAs, a hallmark of obesity, may contribute to the clinically observed cardiac remodeling of obese patients, which may predispose these individuals to AF. It has been suggested that rodents are not a well suited model to study the effects of biofactors from epicardial adipose tissue[234]. Therefore, our studies were conducted with the use of a large animal model: the ovine. Unlike rodents or rabbits, the ovine model has a highly heterogeneous epicardial fat distribution with concentrated depots near the posterior left atrium (LA) and left atrial appendage similar to the epicardial adipose depot in humans. Two saturated FAs (SFAs), palmitic acid (PA) and stearic acid (SA) and one mono-unsaturated FA, oleic acid (OA) are the three major FAs in epicardial adipose of the ovine model, and comprise approximately 85% (25%, 35% & 25.5% respectively) of all free FAs found in blood serum[257,258]. Furthermore, compared to controls, changes in SAFFA levels in obese humans and in sheep are quantitatively similar[258-261]. Analogous to epicardial adipose tissue, humans and other large mammals (e.g. dogs and sheep) share complex atrial transverse (t)-tubule structure that is absent in rodent atrial myocytes[84,262]. Recently, it has been shown that the t-tubule network in the atria is remodeled during certain pathological conditions[263]. Given the close anatomical association between epicardial adipose tissue and atrial myocyte t-tubule structure in large mammals, and the potential for modulatory effects of adipocyte released FAs on the myocardium, we hypothesize that FAs, particularly SFAs, will have unique electrophysiological remodeling capabilities on ovine LA myocytes. Therefore, the objective of the second study is to examine the effects of the three major FAs

found in ovine epicardial adipose tissue and blood serum for 24 hours on cultured LA myocyte electrophysiology.

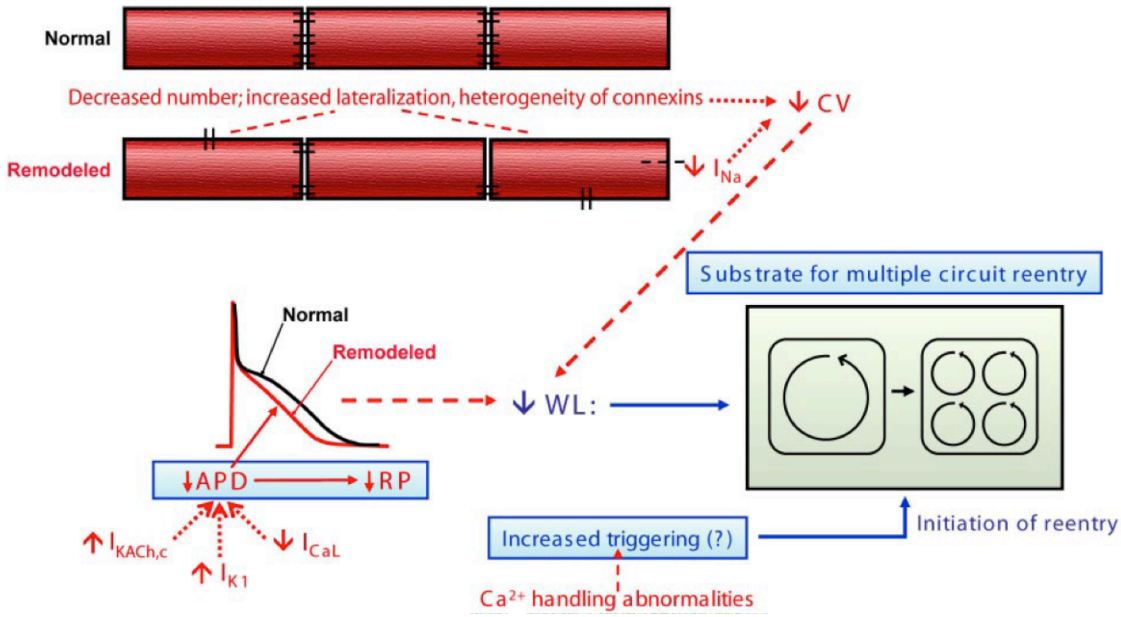

Figure 1.5.1: Pathophysiology of AF promotion by atrial tachycardia remodeling (ATR). The ATR-induced changes in atrial-myocyte electrophysiology that result in AF promotion are indicated in red, with control-cell properties depicted in black. ATR creates a substrate for multiple circuit reentry. The reentry substrate is favored by decreases in refractory period and conduction velocity. The minimum size of a functional reentry circuit is given by the wavelength (or the product of the refractory period and conduction velocity). The shorter the wavelength, the larger the number of reentry circuits that can be maintained simultaneously. When the wavelength is reduced the atria move from the condition shown at the left of the black inset, in which very few circuits are possible and the arrhythmia is unstable, to the situation at the right, for which many more circuits exist and simultaneous extinction of all circuits (which would stop the arrhythmia) is unlikely. Mechanisms governing APD shortening are discussed in the text[5].

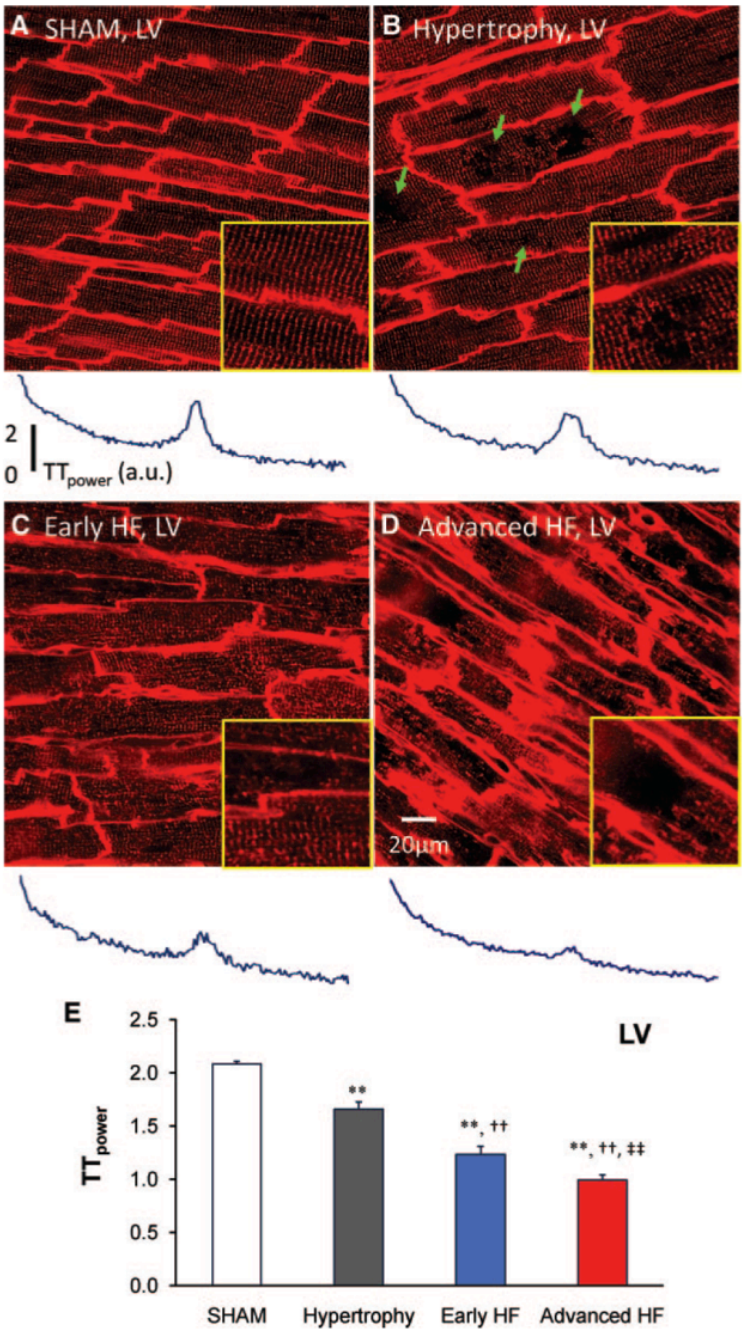

Figure 1.5.2: Progressive t-tubule remodeling of left ventricular myocytes. (A) Representative t-tubule images from left ventricular of age matched sham operated hearts (B) hypertrophy (C) early HF and (D) advanced HF. Bottom graphs show the power spectrums obtained from 2D Fourier transform of the images. (B) At hypertrophy stage, discrete t-tubule loss (green arrows) was often observed with slight t-tubule disorganization, which caused a mild decrease in t-tubule power spectrum. (C) In moderately decompensated heart, left ventricle myocytes exhibited widely impaired t-tubule system and further decrease in t-tubule power spectrum. (D) At advanced HF stage, myocytes lost majority of t-tubules with striated pattern almost vanished, resulting in severe reduction in t-tubule power spectrum. Each yellow-framed inset is a zoomed in view of 40 x 40 µm larger image[2].

Chapter 2

Study 1: The ionic bases of the action potential in isolated mouse cardiac Purkinje cells

2.1 Abstract

Aims: Collecting electrophysiological and molecular data from the murine conduction system presents technical challenges. We have developed an approach for the isolation of murine Purkinje cells (PCs), characterized the major ionic currents and use the ionic data to simulate action potentials (APs) recorded from the isolated PCs.

Methods and Results: Light microscopy was used to isolate and identify PCs from apical and septal cells. Current and voltage clamp techniques were used to record APs and whole cell currents. We simulated a PC action potential, based on our experimental data. APs recorded from PCs were significantly longer than those recorded from ventricular cells. The prominent plateau phase of the PC AP was very negative (~-40mV). Spontaneous activity was observed only in PCs. The inward rectifier current, I_{K1}, demonstrated no significant differences compared to ventricular myocytes (VMs). However, sodium current density was larger, and the voltage-gated potassium current (I_{to}) density was significantly less in PCs compared to myocytes. T-Type Ca^{2+} currents ($I_{Ca\text{-}T}$) were present in PCs but not VMs. Computer simulations suggest that $I_{Ca\text{-}T}$ and cytosolic calcium

diffusion are key determinants of the AP profile recorded in PCs, as compared to VMs.

Conclusions: Our study provides the first comprehensive ionic profile of the murine PCs. The data show unique features of PC ionic mechanisms that govern its excitation process. Experimental data and numerical modeling results suggest that a smaller I_{to} and the presence of the $I_{Ca\text{-}T}$ are primarily responsible for the longer and relatively negative plateau phase of the PC AP.

Keywords: Purkinje cell; specialized conduction system; atrio-ventricular node; action potential duration; Ventricular myocyte

Abbreviations:

AP: action potential;

APD: action potential duration;

SCS = specialized conduction system;

AV node = atrio-ventricular node;

PCs = Purkinje cells;

GFP = green florescent protein;

WT = wild type;

TTX = tetrodotoxin;

Ventricular myocyte = VM

2.2 Introduction

The specialized conduction system (SCS) of the myocardium is important for coordinating cardiac excitation. Components of the SCS in the ventricular myocardium include the atrio-ventricular (AV) node, the His bundle and associated left and right branches, and the cardiac Purkinje fiber network[264]. There is an absolute requirement for precision in the pathway of the conduction of cardiac impulse through the SCS, and deviations therein can be arrhythmogenic and have been associated with various fatal cardiac arrhythmias[265]. Cells within the Purkinje fiber network (Purkinje cells; PCs) distribute the cardiac electrical impulse rapidly and efficiently throughout the ventricular myocardium thereby ensuring effective synchronization of ventricular contraction. Given the role of PCs in the cardiac conduction system, a thorough understanding of excitation in PCs is very important.

The ionic bases of excitation have been investigated by taking advantage of available genetically engineered murine models[266]. Such studies have provided valuable information on the molecular bases of excitation in the working myocardium of the mouse heart, notwithstanding the inherent limitations[266,267]. Compared to the working myocardium, the size of the Purkinje fiber network is very small; consequently, available data on the electrophysiology of mouse SCS is limited, and most of our current knowledge is based on data obtained from immunohistochemistry and from optical mapping of excitation[56,268,269]. In a previous study, action potential (AP) properties in the right bundle branch and Purkinje fiber network were characterized in the mouse using the microelectrode

technique[264]. Results of that study were subsequently confirmed in current-clamp experiments in cells isolated from wild type (WT) and Cx40GFP$^{/+}$ mice[56,268,269]. To our knowledge, there is presently no data in literature on the major ionic currents that underlie excitation in mouse cardiac PCs.

In this study we report, for the first time, basic properties of the major ionic currents in PCs isolated from mouse hearts. Comparisons were made between currents recorded from PCs and from myocytes isolated from septal and apical regions of the ventricle. Using the ionic current data, we developed a mouse PC model by modifying an existing ventricular myocyte model[270]. The PC model was used to investigate the key ionic determinants of the unique AP morphology of the mouse PC.

2.3 Results

2.3.1 Morphology of murine Purkinje cells and ventricular myocytes

We studied, comparatively, morphological features of isolated cardiac PCs and myocytes. PCs were readily distinguishable from myocytes (Figure 2.3.1); although PCs had striations similar to myocytes (Figure 2.3.1A; a & b), they were spindle-shaped, longer, and have a higher length-to-width ratio than myocytes (Table 2.5.1). Lateral membranes of PCs had no obvious cell-cell contact points or “steps” (arrow heads, Figure 1A, b). These features were also evident in PCs isolated from Cx40EGFP$^{/+}$ mouse [271] (Figure 2.3.1A, c & d),

During cell isolation from Cx40GFP$^{/+}$ mice, a small percentage of cells positive for GFP had morphological features atypical for PCs (Figure 2.3.1A, e &

f). On the average, the cells were wider than PCs and had “steps” on lateral membranes (arrows in Figure 2.3.1A, e), features reminiscent of myocytes. We further investigated these cells using confocal imaging of the ventricular endocardium of Cx40GFP$^{/+}$ mice (Figure 2.3.1B). GFP fluorescence of Purkinje fibers was easily identifiable in the endocardial surfaces of the right ventricle. Regions of interest in Figure 2.3.1B (rectangles marked a, b and c) have been enlarged in Figure 1C. Again, whereas Purkinje fibers (marked P) are positive for GFP, myocytes (marked M) are not (Figure 2.3.1C, a), even with further digital enhancement (Figure 2.3.1C, a*). Note that the shape of cells within Purkinje fibers (Figure 2.3.1C, b & c) is consistent with the shape of isolated PCs. Importantly, note that as fibers make contact with the myocardium, cells within the fibers have “steps” on lateral membranes (Figure 2.3.1C, c) reminiscent of myocytes. We will refer to these as transitional cells. As would be expected, the yield of transitional cells was quite low. In the present study, we focused our

electrophysiological investigations only on PCs, with the morphology depicted in Figure 2.3.1A,a.

2.3.2 Passive and active properties of PCs

All electrophysiology experiments were conducted using cells isolated from wild type mice. Compared to the ventricular myocytes, PCs had smaller membrane capacitance, consistent with the smaller cell size and a lack of t-tubules (Table 2.3.1). The resting membrane potential was not significantly different between PCs and myocytes (Table 2.3.1). A characterization of action

potential properties (in PCs, septal and apical myocytes (Figure 2.3.2A)) is a necessary first step in the study the ionic mechanisms underlying excitation. Evoked action potentials in PCs (n=7) (1 Hz) were significantly longer (action potential duration at 70% and 90% repolarization, $APD_{70,90}$; $p<0.05$), and maximum upstroke velocity (dV/dt_{max}) was higher ($p<0.05$) than in septal (n=7) and apical (n=7) myocytes (Table 2.5.5). At 10 Hz PC APDs were abbreviated, whereas apical APD was prolonged, APD_{90} was not significantly different between the two cell types. Isolated PCs demonstrating pacemaker activity were also observed (n=6, Figure 2.3.2B). In addition, paced PCs exhibited early-afterdepolarizations (EADs, 4 out of 7, Figure 2.3.2C), but not observed in septal or apical myocytes.

2.3.3 Ionic currents in isolated murine PCs and ventricular myocytes

PCs utilized for electrophysiology were identified by their distinct cell morphology and, in some instances, by the presence of spontaneous electrical oscillations. In these experiments, we focused our investigations the Hyperpolarization-activated pacemaker current (I_f), the inward rectifier current (I_{K1}), components of depolarization activated potassium (K_v) currents, the L-type ($I_{Ca,L}$) and the T-type ($I_{Ca,T}$) calcium currents and the sodium current (I_{Na}).

Hyperpolarization-activated and inward rectifier currents

Properties of I_f recorded from mouse PCs are shown in Figure 2.3.3 (A, B). Hyperpolarizing pulses (inset) resulted in slowly activating, Cs (5 mM)–

sensitive currents (Figure 2.3.3A), with properties consistent with I_f[73]. Average I_f density/voltage plot in PCs is shown in Figure 3B (n=3). I_{K1} was studied as ramp-generated (1.5 mV/sec; -100 to 0 mV), Ba^{2+} (1mM)-sensitive currents[272,273] (Figure 2.3.3C and D). Representative currents in control and in the presence of Ba^{2+} are shown in Figure 2.3.3C. For comparison, average Ba^{2+}-sensitive currents in PCs, septal and apical cells are shown in Figure 2.3.3D. Peak inward current density at -100 mV was -2.80±0.5 pA/pF (n=6) for PCs, and -2.09±0.35 pA/pF (n=7) and -2.06±0.29 pA/pF (n=7) respectively for septal and apical myocytes; I_{K1} peak inward and outward current density was not significantly different between the three cell types.

Depolarization activated potassium currents

Depolarization-activated potassium currents were characterized as previously described[43]. 5-second depolarizing voltage-clamp pulses were applied from a holding potential of -70 mV, in the presence of TTX (30 μM) and nifedipine (5 μM) to inhibit, respectively, the fast voltage-gated sodium (I_{Na}) and the $I_{Ca,L}$. Representative, normalized current traces and average peak current density/voltage plots are shown in Figure 2.3.4A. Analysis of kinetics of current decay (at +40 mV) were used to determine individual components of the activated currents; $I_{to,fast}$ ($I_{to,f}$), $I_{to,slow}$ ($I_{to,s}$), $I_{K,slow}$ and $I_{steady\ state}$ (I_{ss})[43]. Figure 2.3.4B (left panel) are representative traces recorded in the three cell types accompanied by their respective superimposed fits of current inactivation. Traces were fitted with two (PCs and apical cells) and three (septal cells) exponential

decay functions. Figure 2.3.4B (right panel) is the voltage-dependence of the time constants (τ) of current inactivation. Details of the exponential fits are shown in Table 2.3.2. Values of τ suggest that PCs and apical myocytes have $I_{to,f}$ and $I_{K,slow}$, respectively, τ_1, τ_2, and that septal myocytes have an additional component, presumably $I_{to,s}$. The magnitude of steady state current (I_{ss}) was similar in all cell types.

Voltage-gated calcium and sodium currents

$I_{Ca,L}$ and $I_{Ca,T}$ currents in PCs are illustrated in Figure 5A. The two currents were separated by using two holding potentials (-50 mV and -90 mV). Representative traces of peak $I_{Ca,T}$ (at -50 mV) and $I_{Ca,L}$ (-10 mV) densities are shown as an inset. Figure 2.3.5A (right) is the voltage-dependence of $I_{Ca,L}$ and $I_{Ca,T}$ in PCs. Peak $I_{Ca,T}$ and $I_{Ca,L}$ densities in PCs averaged -0.61±0.16 pA/pF, n=6, N=3 and -3.75±1.32 pA/pF, n=5, N=3, respectively. The L-type calcium currents in septal and apical myocytes are shown in Figure 5B. We could not record any $I_{Ca,T}$ in apical or septal myocytes, consistent with previous reports[274,275]. $I_{Ca,L}$ density was largest in apical cells and smallest in PCs ($p<0.05$). Peak $I_{Ca,L}$ density values were -3.75±1.32 pA/pF, -5.3±0.67 pA/pF, -7.52±0.76 pA/pF, respectively for PCs, septal and apical cells. We also examined I_{Na} density in PCs and in apical myocytes (Figure 2.3.5C). From a holding potential of -160 mV, 300 msec pulses were applied from -100 mV to 0 mV in 5 mV steps. Figure 5C shows mean current density of I_{Na} PCs (n=7) and apical myocytes (n=4). Representative traces are shown in the inset. I_{Na} density was

significantly larger at several applied voltages in PCs when compared to apical myocytes ($p \leq 0.005$, from -50 to -20 mV).

2.3.4 Numerical modeling results

Numerical simulations were conducted to gain further insight into the ionic mechanisms of the mouse PC action potential. Figure 2.3.6A is a schematic of the newly developed PC numerical model with the sub-cellular compartments and ionic currents. The model consists of a radial spatiotemporal Ca^{2+} diffusion process between sub-sarcolemmal (subSL) and sub-sarcoplasmic reticulum (subSR) compartments (two-way arrows). PCs are devoid of t-tubules, which leads to a rather distinct calcium activation process in which calcium ions have to diffuse through the cytoplasm to reach the SR before they trigger calcium-induced-calcium-release (CICR). Therefore, we have implemented a simplistic cytosolic calcium diffusion process to obtain more realistic calcium dynamics in our model (see details in the online supplement). Figure 2.3.6B shows APs elicited in PCs by 1Hz stimulus in experiments and in the model. In the PCs, the AP was characterized by a higher maximum upstroke velocity (dV/dt_{max}), greater AP amplitude. Similar to apical and septal myocytes, PCs have a low voltage plateau (Figure 2.3.2A, see also Figure 2.5.8). The ventricular myocyte model (VM) by Li et al.[270] was also adjusted based on the experimental data as shown in the Appendix. Next, we attempted to delineate the contributions of I_{CaT} and cytosolic calcium diffusion, in order to account for the AP morphology differences between apical myocyte versus the PC. When I_{CaT} was blocked completely in the

PC model, the low-voltage plateau in the action potential disappeared (Figure 2.3.6C) and the AP was significantly shortened (APD_{90} reduced by 25%). Partial blockade of I_{CaT} caused a proportional shortening of APD plateau phase (data not shown).

Several factors control the rise time and decay time of calcium transients in our PC model. These included the extrusion of $[Ca^{2+}]_{subSL}$ by NCX, uptake of $[Ca^{2+}]_{subSL}$ by SERCA, and Ca^{2+} cytosolic diffusion velocity. We kept the first two parameters untouched and altered only the diffusion velocity by varying the spatial diffusion coefficient, D_{Ca}. This way, we could vary the time to peak (T_p) without significantly altering the total time of calcium transient. As shown in Figure 2.3.7A (inset), the APD_{80} was prolonged monotonically with the increase in T_p. The slower calcium transient produced more pronounced plateau in the Purkinje AP (red trace in Fig. 2.3.7A). To study the contribution of calcium diffusion on the AP morphology, we compared the performance of the model with and without Ca^{2+} diffusion. The amplitude of $[Ca^{2+}]_i$ transients was maintained at the same level in both models (Figure 2.3.7B top panel). The spatial diffusion caused slower Ca^{2+} transients, resulting in AP prolongation with the characteristic low-voltage hump (Figure 2.3.7B). In the model without Ca^{2+} diffusion, $[Ca^{2+}]_i$ transients were faster and the AP lacked a prominent plateau. Additional results and complete methodology of the numerical simulations are found in the Appendix.

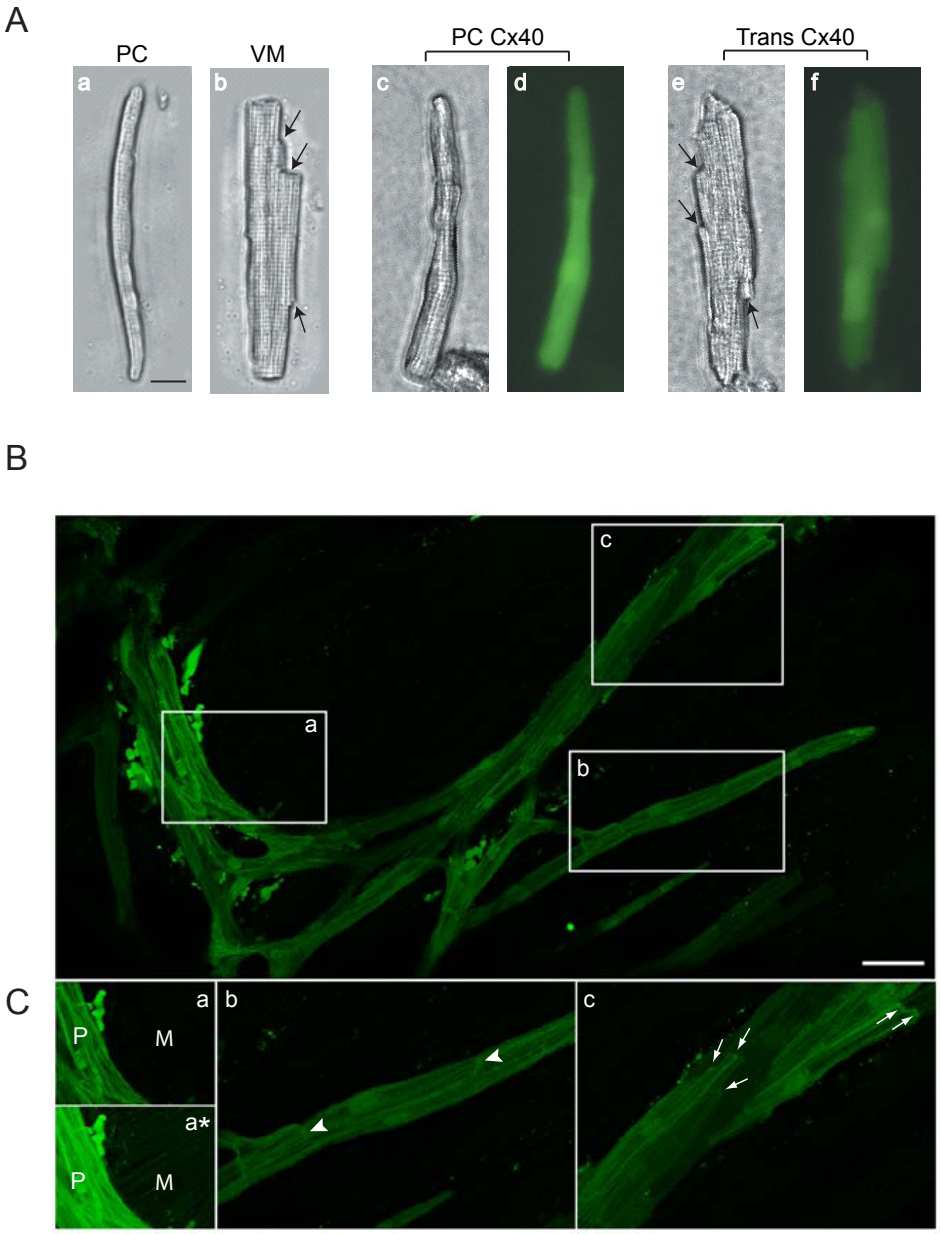

Figure 2.3.1: Morphology of a Purkinje cell (PC) and ventricular myocytes isolated from the murine myocardium. Panel A: Photomicrographs of an isolated Purkinje cell (PC; a) and ventricular myocyte (VM; b) from a wild type mouse heart. For comparison, the panel shows an isolated PC (c) from Cx40 GFP mouse (PC Cx40), where PCs were identifiable by the expression of GFP (d). Phase contrast images of cells expressing GFP (e & f) with "steps" in the lateral membrane (arrows), similar to ventricular myocytes. These were identified as transitional cells (trans Cx40). Scale bar = 20 µM Panel B: GFP-positive Purkinje fibers on right ventricular endocardium. (a), (b) and (c) have been enlarged in panel C. Panel C: (a) Purkinje fibers (P), but not myocytes (M), are positive for GFP, (M), even with further digital enhancement show below (a*). Note regions of contact in b and c; arrowheads in subpanel b and arrows in subpanel c. Transitional cells in subpanel c have steps in lateral membranes[1].

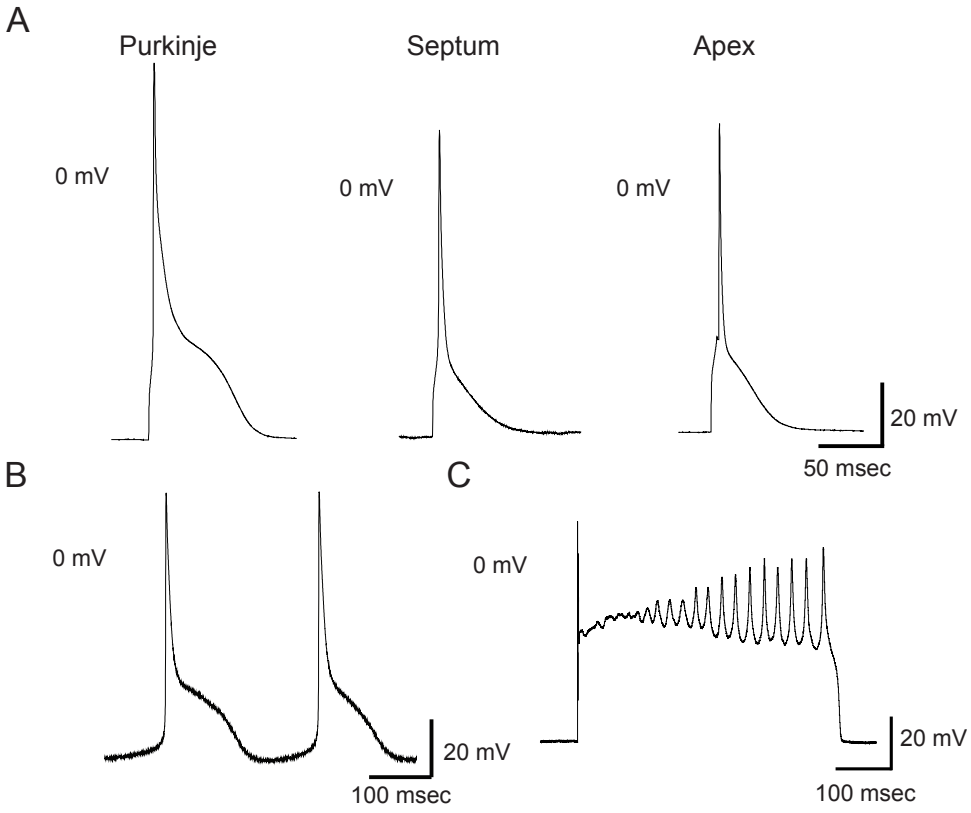

Figure 2.3.2: Action potential characteristics of murine PCs and of ventricular septal and apical myocytes. Panel A (from left to right): Representative traces of action potential morphologies of PCs (n=7), septal (n=7) myocytes and apical (n=7) myocytes. Panel B: Pacemaker activity demonstrated in isolated Purkinje cells (n=6). Panel C: A representative EAD recording in a PC[1].

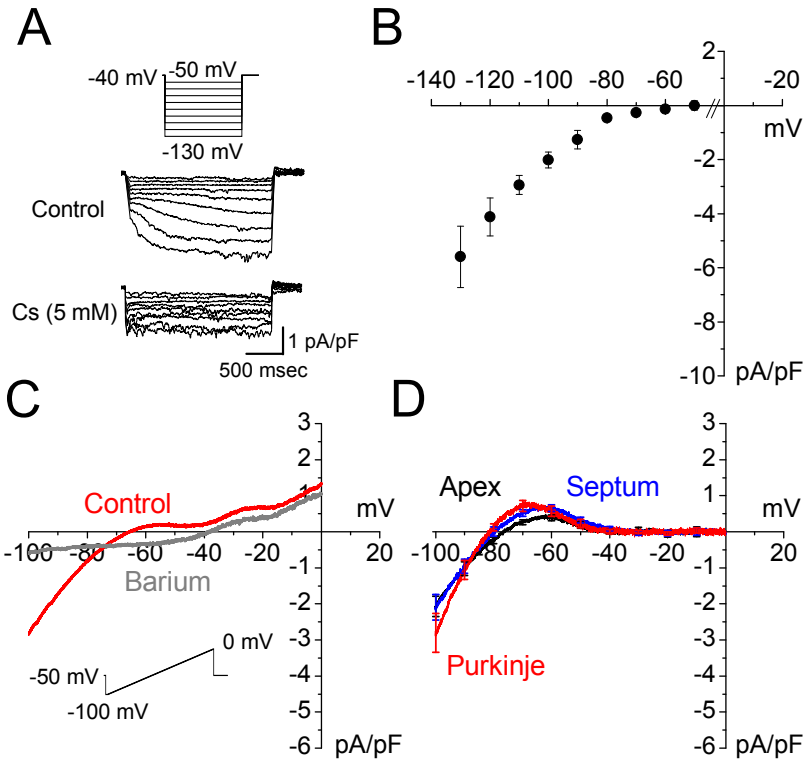

Figure 2.3.3: Hyperpolarization-activated (I_f) and inward rectifier (I_{K1}) currents in PCs. Panel A: Representative currents recorded from all three cell types. Voltage protocol utilized to elicit I_f (upper). Currents recorded in the absence (middle) and presence of 5 mM cesium (bottom). Panel B: I_f peak current density-voltage relationship in PCs (n=3). Panel C: Representative recording of I_{K1} in a PC absence (red) and presence of 1mM Ba^{2+} (black). Voltage protocol is shown as inset). Panel D: Current density-voltage (I-V) relationships of Ba^{2+} sensitive currents (I_{K1}) in PCs (red, n=6), septal myocytes (blue, n=7) and apical myocytes (black, n=7) [1].

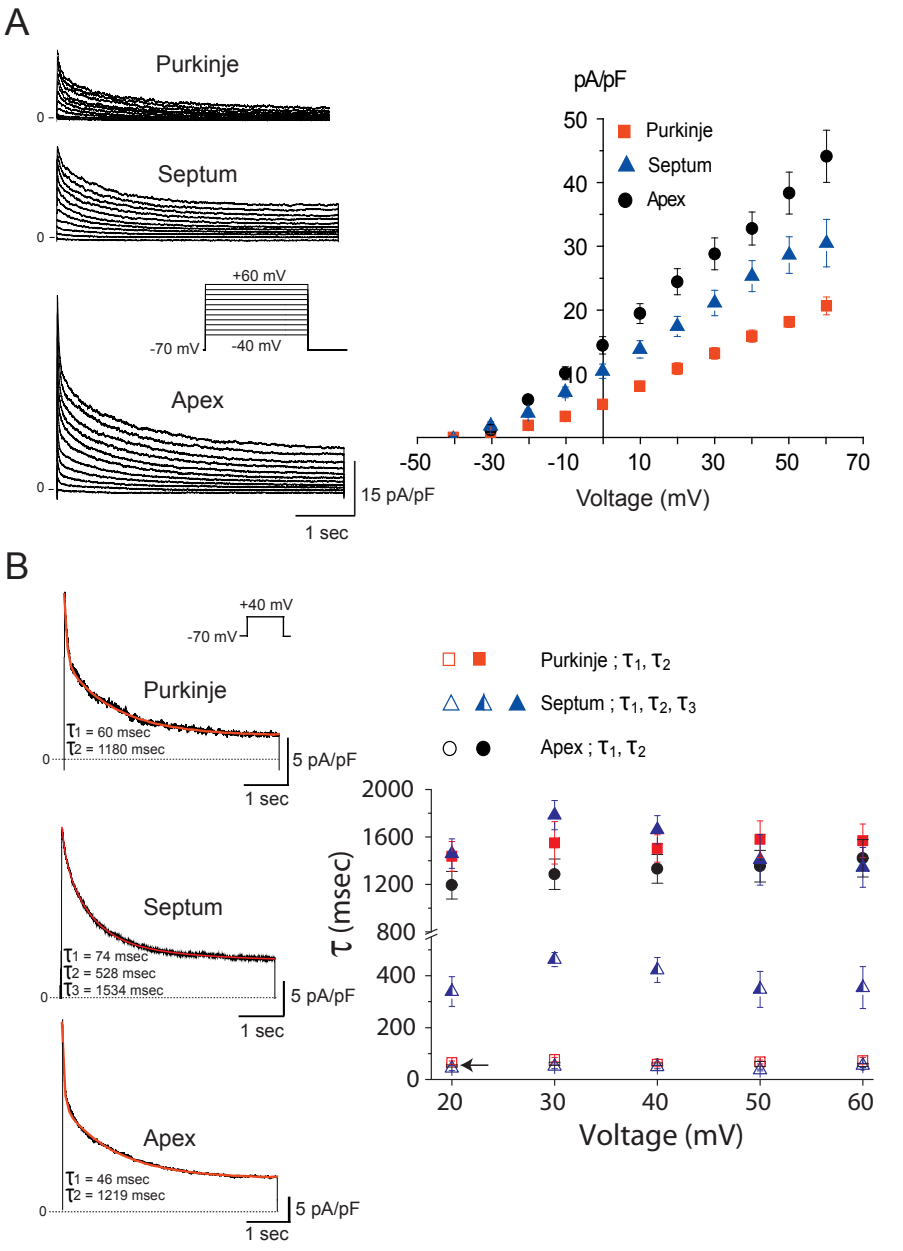

Figure 2.3.4: Depolarization activated potassium currents in isolated cells. Panel A: Current traces following membrane depolarizations from -40 mV to +60 mV (holding potential = -70 mV). Top panel: PCs. Middle panel: septal Cell. Bottom panel: apical cell. Right. I-V relationships in PCs (red, n=6), septal myocytes (blue, n=6) and apical myocytes (black, n=7). Inset: voltage protocol. Panel B: Exponential fits to currents in isolated myocytes. Left panel: PCs, apical myocytes and septal myocytes (inset: voltage protocol). Right panel: Time constants of current inactivation plotted as a function of voltage (nested apical τ1 is indicated by arrow). PCs and apical myocytes were fit with a second order exponential decay function while septal myocytes were fit with a third order exponential decay function[1].

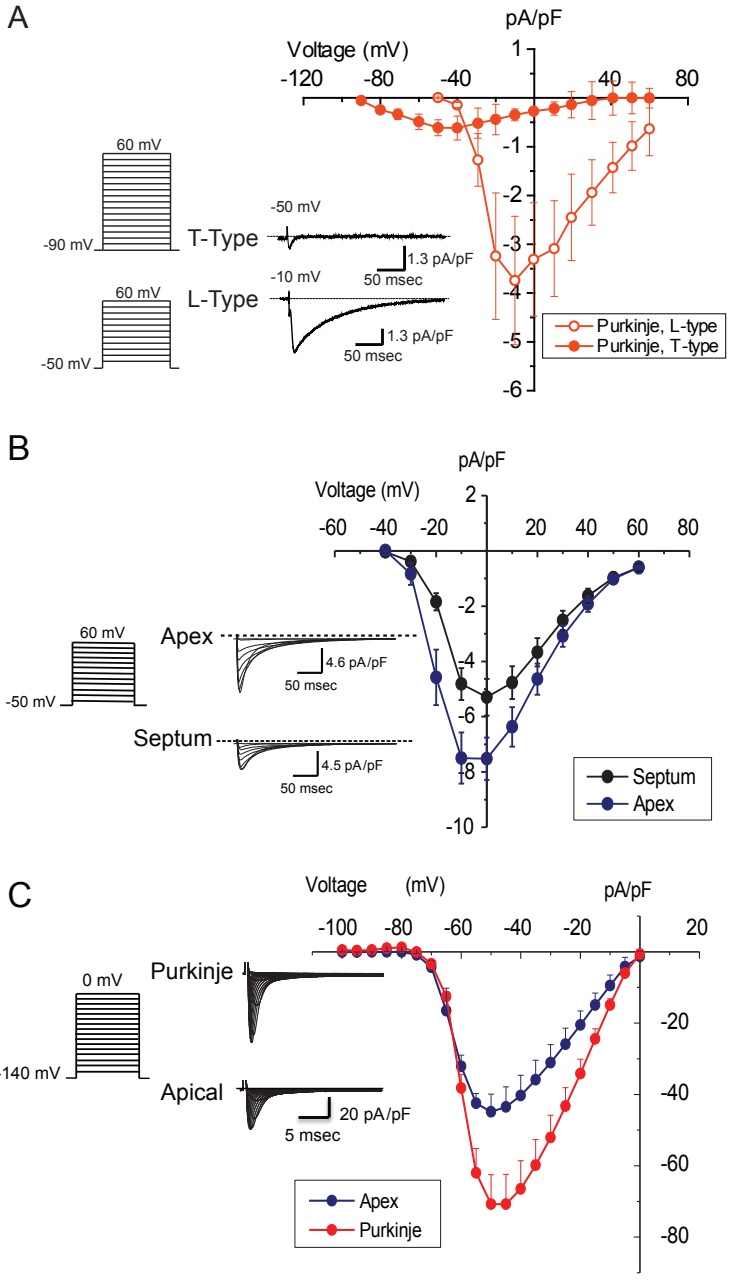

Figure 2.3.5: Calcium and Sodium Currents in PCs and myocytes. Panel A: (inset) voltage protocol and representative traces demonstrating the subtraction to isolate T type currents for PCs. I-V relationship of T and L type Calcium currents in PCs. Panel B: (inset) Representative traces for apical and septal myocytes. I-V relationship of $I_{Ca\text{-}L}$ for septal (black, n=6) and apical (blue, n=6) myocytes. Panel C: (inset) voltage protocol and (middle) representative traces of I_{Na} recorded in a PC and an apical myocyte. (Right) I-V relationship of I_{Na} in PCs (n=7) and apical myocytes (n=4) [1].

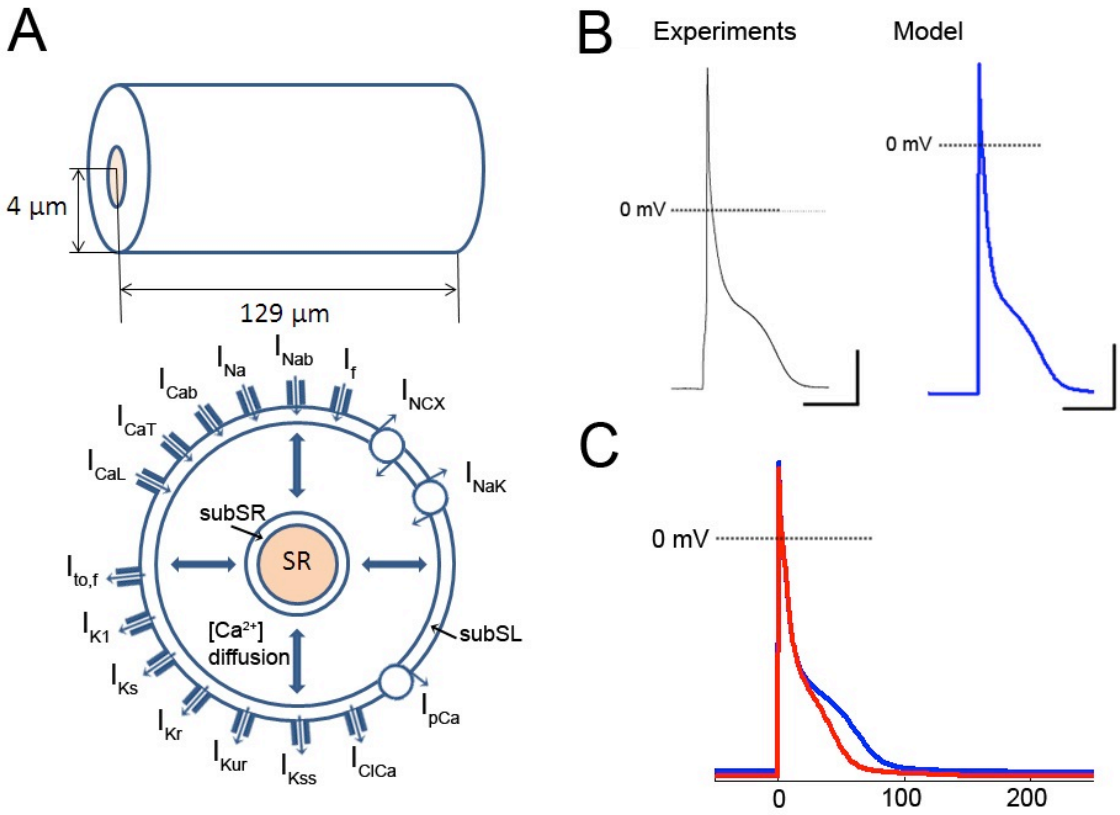

Figure 2.3.6: Morphologically realistic numerical model of a PC. Panel A: Schematic of the PC numerical model showing subcellular compartments (sub-sarcolemmal (subSL) and sub-sarcoplasmic reticulum (subSR)) and the ionic currents in the cell. The model consists of radial spatiotemporal Ca^{2+} diffusion between subSL and subSR compartments as shown by the two-way arrows. Panel B: Action potentials (at 1 Hz) in PCs elicited in experiments and in the model. Horizontal and vertical scale bars represent 50 ms and 20 mV, respectively. Panel C: I_{CaT} blockade in the PC model resulted in a significant reduction of plateau phase (red) and abbreviation of APD.

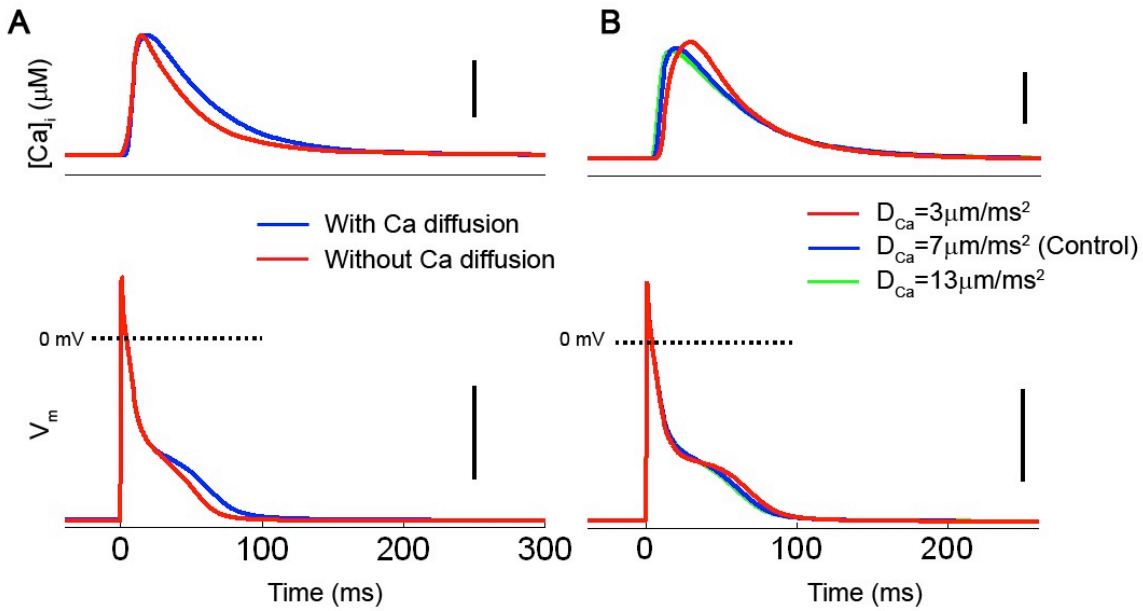

Figure 2.3.7: Role of cytosolic Ca diffusion in AP morphology of mouse PC. Panel A: Slowing of Ca transients by decreasing diffusion coefficient (D_{Ca}) produced more pronounced plateau in the AP. Inset: APD80 increased monotonically with increase in $[Ca]_i$ time to peak (T_p). Panel B: Comparison between the PC model AP with and without calcium diffusion. Spatiotemporal $[Ca]_i$ diffusion resulted in slower calcium transients which prolonged the AP. PC model without $[Ca]_i$ diffusion exhibited faster transients and no plateau in the AP. Vertical scale bars represent 0.4 μM (top panels) and 40 mV (bottom panels) [1].

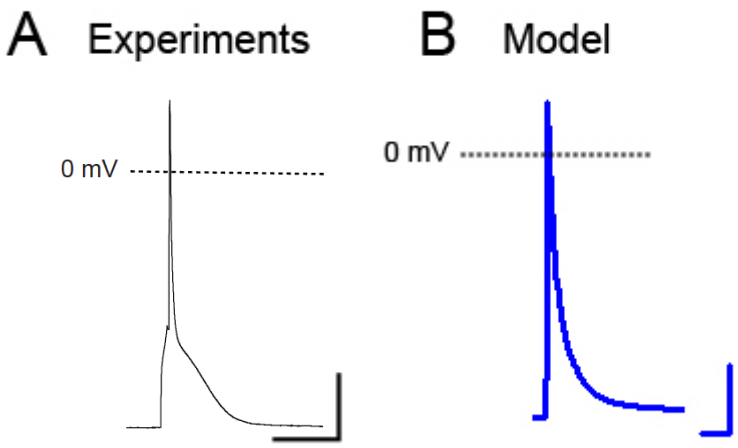

Figure 2.3.8: (S10)Sample action potentials in apex ventricular myocytes recorded experimentaly (left) and obtained by using the modified VM model (right). Horizontal and vertical scale bars represent 50 ms and 20 mV, respectively[1].

	Length (μm)	Width (μm)	Cap (pF)	RMP (mV)	dV/dt (V/sec)	APD_{50} (msec)	APD_{70} (msec)	APD_{90} (msec)	MDP (mV)
Purkinje	129±7*	8±0.3*	79.9±4*	-82±1	212±15#	4.7±0.3	14.4±1.6#	68.6±5# 54±4^	- 72±1
Septum	110±2	25±0.7	131±8.7	-79±1.6	160±21	4.7±0.4	9.5±1.0	45±3.8 ND^	--
Apex	104±2	27±0.9	167±13. 9	-79±0.3	114±12.9	3.3±0.6	9.3±2.2	44.1±4.9 51±7^	--

Table 2.3.1: Morphology and Action Potential Characteristics in Isolated Purkinje, Septal and Apical Myocytes at 1 Hz (^APD_{90} at 10 Hz; *P<0.001; #P<0.05) [1].

		I_{peak}	$I_{to,f}$	$I_{to,s}$	$I_{K,slow}$	I_{SS}
Purkinje	τ (msec)	--	58.4±9.4	--	1502±115	--
	pA/pF	18.7±2.7*	4.2±0.6	--	8.9±1.8	5.7±0.9
Septum	τ (msec)	--	48.6±7.1	412±40.4	1834±200	--
	pA/pF	25.7±2.5	3.8±1.0	5.9±1.6	10.7±1.4	5.3±0.6
Apex	τ (msec)	--	58.6±4.8	--	1331±121	--
	pA/pF	32.4±2.6	13±1.5	--	13.2±1.3	6.2±0.9

Table 2.3.2: Kinetic Analysis of Depolarization Activated Potassium Currents in Isolated Myocytes (*P<0.001) [1].

2.4 Discussion

We have carried out comprehensive current- and voltage-clamp experiments as well as numerical modeling of excitation of mouse PCs. To our knowledge, this is the first report of such data in the literature. The main findings from the experiments and numerical modeling suggest that PCs have a smaller I_{to} density which may, in part, be responsible for the longer PC APD. Furthermore, our simulations suggest that the presence of I_{CaT} give is important in defining the PC action potential morphology.

Morphology of isolated murine Purkinje cells and ventricular myocytes

Based on light and electron microscopy morphological analyses of fibers/cells from a variety of species, three types of PCs have been described[20,276]; ungulates (group I), carnivores and primates (group II) and rodents (group III). In group III, PCs are smaller in size than myocytes, and are cylindrical in shape, consistent with our findings. The light and confocal microscopy data demonstrate that “transitional” PCs can make side-to-side contacts, presumably at the Purkinje-Muscle junctions.

Ionic bases of excitation in mouse Purkinje cells – experimental and numerical insights

Heterogeneity in AP morphology and ionic currents are established characteristics of myocardial cells[43,277]. In mouse PCs, APD_{90} values (1 Hz) are ~34% greater compared to in septal or apical cells. The plateau phase of APs in

the canine, ovine as well as the rabbit PCs is relatively more negative in voltage range (~ 0 to -20 mV) compared to ventricular myocytes[26,278,279]. Repolarization in phase 2 of PCs is more negative (~ -40 mV; see Figure 2A) in mouse PCs when compared to other species (see Verkerk et al, 1999[280]). It is noteworthy that phase 2 repolarization in murine ventricular myocytes are relatively more negative than what has been demonstrated in other species. It is possible that the specific densities of murine ITO and calcium currents in the PCs and VMs might explain this low plateau phase[280].

The voltage-dependent activation properties of I_f imply that the current should play a role in the spontaneously generated action potentials in PCs. Nevertheless, we cannot rule out contributions from other current mechanisms, including IK_{dd}[281] or calcium waves.[279,282] The molecular correlates of I_f in the rabbit have been identified as HCN2 and HCN4[283]. Further investigations will be required to ascertain the molecular nature of the proteins that underlie I_f in mouse PCs. I_{K1} density in the rabbit[284], sheep[280] and canine[285] PCs are smaller than in myocytes. There were no significant differences in I_{K1} density between mouse PCs and myocytes also consistent with what has been reported previously in human Purkinje versus ventricular cells [286] [287] [288]. It is noteworthy that no significant differences were found in I_{K1} density between mouse atrial and ventricular myocytes[289], and may suggest a peculiarity of this species.

Mouse ventricular myocytes have negligible delayed rectifier potassium currents, I_{Kr} and I_{Ks} (~0.2 pA/pF)[290] and were thus not investigated in the present study. Compared to myocytes, PCs had significantly smaller transient outward

currents. Analyses of current properties show that PCs and apical myocytes have similar kinetics, in which current decay could be fitted with two exponentials, presumably reflecting $I_{to,f}$ and $I_{K,slow}$. In contrast, kinetics of current decay in septal myocytes required three exponentials to be adequately fitted. This would suggest that $I_{to,s}$ (tau of ~400 msec) is a component of the activated currents[43,48]. It might be tempting to speculate that the molecular bases of the transient outward currents in PCs and apical myocytes are similar; however molecular identification of the channel proteins will be required to establish this.

L- and T- type calcium currents are present in mouse PCs. We propose that the T- type channel plays a role in the negative voltage range of phase 2 repolarization. In numerical simulations, only the T-type calcium current was capable of prolonging the APD in PCs. The data suggests that action potential characteristics are attributable to intracellular calcium dynamics and the T-type calcium current. Both components may contribute to the prolonged AP with the low-voltage plateau in the Purkinje cells. Our findings are consistent with changes in action potential morphology following expression in myocytes of α1G, which encodes T-type calcium channel[291]. We show that I_{Na} density in PCs is significantly larger ventricular myocytes. Recently Vassalle et al[292] reported that in the canine cardiac PCs, a slowly inactivating sodium current (I_{Na2}) plays a role in prolonging the plateau of the action potential. We presently cannot rule out this possibility in the murine PC.

Study limitations

Our main objective in this study was to demonstrate the feasibility of recording membrane ionic currents in PCs isolated from wild type mice, without cross breeding with Cx40GFP$^{/+}$ mice. Although we have characterized the major ionic currents, these technically challenging experiments precluded the identification of molecular correlate of the ion channels. Our model assumes a symmetric morphology of a PC with the SR located at the center and consists of a simplistic cytosolic calcium diffusion process. Despite this, it enabled us to study the effects of cytosolic calcium diffusion on the AP morphology of Purkinje cells. We did not consider possible effects of alteration in Ca^{2+}-dependent inactivation of I_{CaL}, which could also further affect the shape of AP plateau. Nonetheless, we were able to speculate that cytosolic spatiotemporal diffusion and the presence of T-type calcium channels are responsible for the peculiar AP morphology. Further characterization of cytosolic calcium diffusion via experiments, and a detailed model development for the same is needed to investigate its putative role in the cell-wide calcium waves and the increased propensity of afterdepolarizations in the Purkinje cells.

Conclusions

We have demonstrated the feasibility of using available mouse models to investigate the molecular underpinnings of excitation in the specialized conduction system. Because this approach does not require cross breeding with the Cx40EGFP$^{/+}$ mouse, less time and resources are needed for such future investigations. Our experimental and numerical modeling data suggests that

cytosolic calcium diffusion and T-type calcium current, alone or in combination, contribute to the prolonged AP with the low-voltage plateau in PCs.

2.5 Methods

Mouse cardiac Purkinje cells and ventricular myocytes were dissociated using Langendorff method as previously described[56]. All procedures were carried out in accordance with the University of Michigan guidelines for animal use and care conformed to the Guide for the Care and Use of Laboratory Animals published by the US National Institutes of Health (NIH Publication 58-23, revised 1996). Experimental details are given in the Online Supplement.

Animals

All investigations carried out in this study conformed to the *Guide for the Care and Use of Laboratory Animals* (NIH Publication no. 85–23, revised 1996).

Cell isolation

Cardiac Purkinje cells and ventricular myocytes were isolated using a procedure previously described[56,268]. Briefly, mice (2-5 months old) were heparinized (0.2-0.5 ml heparin (100 IU/ml i.p.) and then anesthetized with a mixture of ketamine (116 mg/Kg) and acepromazine (11mg/Kg) i.p. The heart was quickly excised, placed in cardioplegic solution containing (in mmol/L): Glucose 280, KCl 13.44, NaHCO3 12.6, Mannitol 34[293]. The aorta was cannulated and retrogradely perfused at 37°C for 4 min with a Ca^{2+}-free solution (perfusion buffer) containing

(in mmol/L): 113 NaCl, 4.7 KCl, 1.2 $MgSO_4$, 0.6 Na_2HPO_4, 0.6 KH_2PO_4, 10 $KHCO_3$, 12 $NaHCO_3$, 10 HEPES, 10 2.3-butanedione monoxime (BDM, Sigma), 30 taurine, and 5.5 glucose. For enzymatic digestion, collagenase type II (Worthington; 773.4 u/ml), trypsin (0.14 mg/ml), and $CaCl_2$ (12.5 µmol/L) were added to the perfusion buffer, and digestion carried out for ~5 mins. Following digestion the ventricles were cut open and Purkinje fibers were extracted using micropipettes coupled to a suction device, or shaved off the endocardial surfaces of the ventricles. Ventricular myocytes from the apex and septum were isolated as described previously by Xu et al[43]. Cells were isolated by gentle teasing and mechanical agitation of Purkinje fibers or muscle tissue in a stopping buffer (perfusion buffer plus 10% fetal bovine serum and 12.5 µmol/L $CaCl_2$). Subsequently, the Ca^{2+} concentration was gradually increased to 1.0 mmol/L with approximately 5 min of incubation between steps at 37 ^oC. After calcium reintroduction the cells were spun at 1000 rpm for 10 seconds and then re-suspended in Tyrode solution of the following composition (mM): NaCl 148, KCl 5.4, $MgCl_2$ 1.0, $CaCl_2$ 1.0, NaH_2PO_4 0.4, glucose 5.5, HEPES 15, pH 7.4 (NaOH). Cells were used for electrophysiological recording within 8 hours after isolation. Three to five mice were used for each set of experiments reported in this study.

Electrophysiology

Borosilicate glass electrodes for cellular electrophysiology experiments were pulled with a Brown-Flaming puller (model P-97), yielding a tip resistance of 3-5 MΩ when filled with pipette solution. Data were recorded using a Multiclamp-

700B and/or Axopatch-200B amplifiers and the pClamp10 suite of programs (Molecular Devices, Inc., Sunnyvale, CA). Voltage-clamp experiments were carried out at room temperature (22-28 ^{o}C). I_{to} and action potentials were recorded at 37 ^{o}C.

Whole-cell current-clamp

Action potentials were elicited in quiescent cells using a train of 20, 5-msec stimuli (1 and 10 Hz; DS8000 Digital Stimulator; World Precision Instruments). Resting membrane potential, action potential duration at 70 and 90% repolarization ($APD_{70,90}$) and dV/dt_{max} were analyzed as previously published[56]. Quiescent cells were chosen for action potential pacing protocols. Pacemaker activity in PC cells was investigated in cells that demonstrated stable diastolic depolarization.

External solution (mmol/L): NaCl 148, NaH_2PO_4 0.4, $MgCl_2$ 1, Glucose 5.5, KCl 5.4, $CaCl_2$ 1.0, HEPES 15; pH 7.4 (NaOH).

Pipette filling solution (mmol/L): KCl 148, $MgCl_2$ 1, EGTA 0, HEPES 5, Creatine 2, K_2-ATP 5, Phosphocreatine 5; pH 7.2 (KOH).

Whole-cell voltage-clamp

Hyperpolarization-activated pacemaker current, I_f

External solutions (mmol/L): NaCl 148, NaH_2PO_4 0.4, $MgCl_2$ 1, Glucose 5.5, KCl 5.4, $CaCl_2$ 1.0, HEPES 15. For I_{K1} measurement, 5 μM nifedipine was added to

block I_{CaL} channels and the Ca^{2+}-sensitive I_{Cl}. $BaCl_2$ (0.4-1 mmol/L) was used to block I_{K1}.

Pipette filling solution (mmol/L): KCl 148, $MgCl_2$ 1, EGTA 5, HEPES 5, Creatine 2, K_2-ATP 5, Phosphocreatine 5; pH 7.2 (KOH).

Protocol: A ramp protocol with a velocity of 1.5 mV/sec was used between -100 to +20 mV from a holding of -50 mV.

Inward rectifier current, I_{K1}

External solutions (mmol/L): NaCl 148, NaH_2PO_4 0.4, $MgCl_2$ 1, Glucose 5.5, KCl 5.4, $CaCl_2$ 1.0, HEPES 15.

*Pipette filling solution (mmol/L):*KCl 148, $MgCl_2$ 1, EGTA 5, HEPES 5, Creatine 2, ATP 5, Phosphocreatine 5; pH 7.2 (KOH).

Protocol: A ramp protocol with a velocity of 1.5 mV/sec was used between -100 to +20 mV from a holding of -50 mV.

For I_{K1} measurement, 5 µmol/L nifedipine was added to block I_{CaL} channels and the Ca^{2+}-sensitive I_{Cl}. $BaCl_2$ (1 mmol/L) was used to isolate I_{K1} from other background currents[273,293].

Depolarization-activated potassium currents

External solutions (mmol/L): NaCl 148, NaH_2PO_4 0.4, $MgCl_2$ 1, Glucose 5.5, KCl 5.4, $CaCl_2$ 1.0, HEPES 15 (pH 7.4 with NaOH). To block sodium channels and calcium channels 30 µmol/L TTX (Tetrodotoxin) and 5 µmol/L Nifedipine was added to the external solution.

Pipette filling solutuion (mmol/L): KCl 138, EGTA 10, HEPES 10, $MgCl_2$ 1, glucose 5 (pH 7.4 with KOH).

Protocol: Potassium currents were recorded using 5-second depolarizing pulses to potentials between -40 mV and +60 mV from a holding of -70 mV. Voltage steps were in steps of 10 mV at 15 sec intervals[43].

Analysis: To isolate the underlying currents recorded using the protocol described above, the traces with fit with a second or third order exponential decay function as described previously[43,48].

L and T Type Calcium currents

External solutions (mmol/L): NaCl 137, CsCl 5.4, $MgCl_2$ 1, $CaCl_2$ 1.2, HEPES 10, Glucose 10, 4-Aminopyridine (4-AP) 2, (pH 7.35 with NaOH)[294].

Pipette filling solution (mmol/L): CsCl 120, TEA-Cl 20, $MgCl_2$1, MgATP 5, Na_2GTP 0.2, HEPES 10, and EGTA 10 (pH 7.2 with CsOH)[294].

Isolating the T-type current: For L-Type calcium current measurement, myocytes and Purkinje cells were held at –80 mV, and Na^+ currents were inactivated by applying a prepulse to –40 mV for 300 ms before step depolarizing to voltages ranging from –40 to +60 mV for 300 ms[294]. For T-type calcium current, cells were held at -90 mV and TTX (30 μM) was used to block the inward sodium current and stepping the voltage from -90 to +60 mV in steps of 10 mV.

Sodium Current

External Solutions (mmol/L): NaCl 5, $MgCl_2$ 1, $CaCl_2$ 1.0, $CdCl_2$ 0.1, HEPES 20, Glucose 11, CsCl 132.5 (pH = 7.35 with CsOH).

Pipette filling solution (mmol/L): NaCl 5, CsF 135, EGTA 10, MgATP 5, HEPES 5 (pH = 7.2 with CsOH).

Protocol: In order to record sodium currents cells were held at -160 mV followed by depolarizing steps from -100 to -10 mV in 5 mV increments. The duration of the voltage steps were 300 msec with a 5 second interval between successive voltage steps.

Confocal Imaging of sections of murine ventricle

Mice were anesthetized and heart was excised as described above. The heart was immediately placed in ice-cold cardioplegic solution, cannulated via the aorta, and perfused with ice-cold phosphate buffered solution (PBS) until all blood had been cleared. Right ventricle free wall and septum were dissected away from the heart and placed in ice cold PBS. Sections of the whole heart were imaged using a Nikon Eclipse Ti (Nikon Inc, Japan) inverted confocal microscope. GFP fluorescence was detected following excitation with a 488-nm argon laser and a 40X oil-immersion objective lens (Plan Fluor) with a numerical aperture (NA) of 1.30.

Statistical Analyses

Student *t* test was used to compare normally distributed variables. Cross tabulation with Fischer's exact test was used for categorical variables. The data are presented as means ± SE. We used the SPSS (version 15.0) or the Origin (version 8.0) statistical packages.

Chapter 3

Study 2: Free fatty acid effects on the atrial myocardium: Disruption of t-tubular architecture and remodeling of membrane ionic currents

3.1 Abstract

Introduction: Epicardial adiposity and plasma levels of free fatty acids (FFAs) are elevated in obesity, with potential effects on myocardial function. The role of saturated FFAs on impulse generating mechanisms of myocardial cells is not fully understood.

Objective: To determine the mechanisms underlying electrophysiological effects of elevated levels of palmitic (PA), stearic (SA) and oleic (OA) acids on sheep atrial myocytes.

Methods: We used electrophysiological techniques, numerical simulations, biochemistry and optical imaging to examine the effects of acutely (≤ 120 mins) or chronically (24 hrs) applied FFAs on properties of isolated atrial myocytes.

Results: Acute application of FFAs (10 μM of FFA) or adipocyte-conditioned media on myocytes had no significant effects on resting membrane (RMP) or action potential duration (APD; n=15-24). Chronically applied PA did not affect RMP or capacitance (C_m), but abbreviated APD_{30}, and reduced L-type calcium current ($I_{Ca\text{-}L}$) by 30% ($p<0.05$; n=7-12). There were no significant effects on the transient outward (I_{TO}), or the fast voltage-gated sodium currents (I_{Na}).

Chronically applied SA did not alter RMP but reduced C_m ($p<0.05$) and shortened APD at all values of repolarization ($p<0.001$). $I_{Ca\text{-}L\ (peak)}$ and $I_{TO\ (+60mV)}$ were reduced respectively by 60% and 30%. Chronically applied OA did not alter APD or ionic current properties. A human atrial cell model recapitulated SA effects on APD. Chronically applied SA reduced t-tubular staining (Di-8-ANEPPS) in isolated atrial myocytes ($p<0.0001$; n=23).

Conclusions: SA disrupts t-tubular architecture and remodels properties of membrane ionic currents in atrial cells, with potential implications in arrhythmogenesis.

List of Abbreviations:

Atrial fibrillation (AF); free fatty acid (FFA), fatty acid (FA); left atria/atrium (LA); palmitic acid (PA); stearic acid (SA); oleic acid (OA); vehicle control (CTL); action potential (AP); action potential duration (APD); polyunsaturated free fatty acid (PUFFA); saturated fatty acid (SFA); resting membrane potential (RMP); sodium current (I_{Na}); L-type calcium current (I_{CaL}); transient outward potassium currents (I_{TO}); transverse tubule (t-tubule); left ventricular myocyte (LVM)

3.2 Introduction

Studies in humans and animal models show that obesity significantly increases plasma levels of free fatty acids[258,260] as well as overall visceral and epicardial adiposity.[231,236] Increasingly, clinical investigations report a relationship between obesity and atrial fibrillation (AF) risk, as well as in the incidence and/or persistence of AF.[237,239-243] One generally evaluated postulate is that free fatty acids and adipokines (biofactors) are important modulators with potential to remodel the myocardium, which increases the risk of arrhythmogenicity[234-236,239,240,249,261].

A significant portion of the epicardial surface in large mammals is normally covered by adipose tissue,[238-240] and fat cells (adipocytes) may be involved in myocyte-adipocyte cross talk important in the normal function of the myocardium[250,251]. With obesity, extensive fatty infiltration will result in elevated levels of biofactors and potentiated by paracrine and “vasocrine” signaling pathways will overload the myocardium with these biofactors[235,248]. Elevated levels of biofactors may detrimentally alter myocardial function by several mechanisms such as by promoting abnormal impulse initiation mechanisms and by causing atrophy of the surrounding myocardial cells.[248,250,251,261] In fact, in obese men, it has been reported recently that steatosis of the myocardium correlates with epicardial fat, and is an independent contributing factor to myocardial dysfunction. These troubling possibilities have prompted experimental studies in isolated myocytes, results of which in general, show that excess epicardial adiposity, or its biofactors, cause abnormality in myocardial electrical

excitation.[295] However, results from such investigations, which were conducted primarily in rodent and lagomorph animal models, have been inconsistent;[296,297] There are presently no equivalent cellular electrophysiological investigations in humans or in a large animal model.

A very recent study reported changes in atrial histology and size, and significant abnormalities in impulse conduction in the myocardium of an obese sheep model.[298] However, the underlying cellular mechanisms were not determined. Biochemical composition of ovine and human epicardial fat are similar: the predominant fatty acids in epicardial fat depots are the saturated free fatty acids (SFA; palmitic acid and stearic acid), and the mono-unsaturated fatty acid, oleic acid, with a composition respectively of 25%, 35% and 26%.[238,257] There is evidence also that these specific biofactors may be regulated similarly in obese sheep and humans.[258-261] Although the electrophysiological effects of unsaturated fatty acids have been widely studied [254], SFA effects on myocyte electrophysiology are poorly understood. The objective of this study is to examine the effects, as well as the underlying mechanisms, of chronically applied SFAs on atrial myocytes isolated from sheep hearts. Our choice of the ovine model is predicated on the similarity to humans, of the biochemical content of epicardial fat as well as the ionic currents underlying myocardial excitation. The study was carried out using a combination of electrophysiological, biochemical, optical techniques and numerical simulations on myocytes isolated from the left atrium of the sheep.

3.3 Results

Epicardial fat and fatty acid effects on atrial myocyte electrophysiology

3.3.1 Close apposition of adipocytes and myocytes in sheep atrial myocardium

In humans and in large mammals, epicardial fat distribution on the atrial myocardium is considered generally less extensive compared to the distribution on the ventricular epicardium[235,238]. In the left atrium of sheep and human hearts, however, the pulmonary vein region is reported to have extensive fat deposits.[235] Figure 3.3.1(panels A and A1) shows typical features of the epicardial surface of a normal, ~35 kg adult sheep such as those used in the experiments (N=5). The figure shows that the left atrial appendage has significant fat layers, which randomly infiltrate the myocardium as depicted in panels B & B1. The picture in panel B is a high resolution, single image montage, captured automatically as a series of contiguous images using a microscope with a motorized stage (see Methods). In panel B1, islands of mature adipocytes can be seen in close contact with myocytes, with apparently no intervening fascia, as reported for epicardial fat on human ventricular myocardium[238,248]. This proximity of adipocytes to the surrounding myocardial cells will support the contention of adipocyte-myocyte biochemical cross talk, involving biofactors, e.g., fatty acids[235,238]. Thus, excess biofactor production could potentially alter normal cellular electrophysiology. In this study we have focused our electrophysiological analysis using the three free fatty acids- palmitic (PA), stearic (SA) or oleic (OA) acids that are the main components of epicardial fat depots in the ovine model.[237,249]

3.3.2 Fatty acid effects on resting membrane and action potential properties

In all electrophysiology experiments, myocytes were isolated from the left atrial (LA) appendage region of adult sheep hearts (areas depicted in Fig 3.3.1; A & A1). Based on the previously reported effects of acute application of biofactors or adipocyte-conditioned media (ACM; see Methods) on rodent and rabbit myocytes, [253,256,297,299,300] we initially tested the effects of acutely applying SFAs (10 μM) or ACM on the ovine atrial myocytes. Acute (in mins) or short-term (4-6 hrs) application of PA or SA on myocytes had no significant effects on action potential properties (Supplemental Figure 1). Moreover, there were no changes on resting membrane potential (RMP) or whole cell capacitance (data not shown). However, chronic (24 hr) application of ACM significantly abbreviated action potential duration (APD) at 50% (APD50) and at 80% (APD80) repolarization by 52% and 25%, respectively (**$p<0.001$, *$p<0.01$; Supplemental Figure 2). Subsequently, we studied the effects of chronic incubation of myocytes in SFAs (PA, SA) or in OA. PA and OA did not alter passive electrical properties (RMP, cell cap, etc.; Table 3.3.1). SA, similarly, had no effect on RMP but significantly reduced whole cell capacitance (cell cap; *$p<0.05$). The values presented in Table 3.3.1 (i.e. after 24 hrs) were not different from the passive properties collected acutely (0 hrs; data not shown). Fatty acid effects on APD were examined at three values of repolarization (30%, 50% and 80%) and illustrated in Figure 3.3.2. PA significantly reduced APD30 (msec) from 52.7 ± 8.4 to 26.4 ± 8.8; $p<0.05$ (Figure 3.3.2A & B). Incubation of myocytes in SA resulted in a very significant reduction ($p\leq0.001$) of APD at all values measured (Figure 3.3.2C &

D). In contrast to the effects of the SFAs, the mono-unsaturated OA did not alter APD properties at any value of repolarization measured (Figure 3.3.2E & F).

3.3.3 Fatty acid effects on membrane ionic currents

Results from the preceding section show that compared to PA, SA caused more significant changes on the passive and active electrical properties of atrial cells. An examination of free fatty acid effects on major membrane currents was therefore carried out in cells incubated primarily in SA. In these experiments, we examined the effects of chronic application of SA on the fast sodium current (I_{Na}) and the L-type calcium current ($I_{Ca\text{-}L}$), which are the key voltage-gated currents involved in membrane depolarization in atrial cells. SA did not alter I_{Na} current density (Figure 3.3.3A & B), or the voltage dependent activation or inactivation properties (Figure 3.3.3, C). In contrast, SA decreased peak $I_{Ca\text{-}L}$ by ~60% compared to control values (Figure 3.3.3, D & E). Peak $I_{Ca\text{-}L}$ density was reduced from -2.2 ± 0.5 pA/pF to -0.9 ± 0.1 pA/pF (*$p<0.01$). As shown in Figure 3.3.3 F, the reduction of $I_{Ca\text{-}L}$ occurred without changes in voltage-dependent current activation or inactivation properties. We also examined free fatty acid effects on the voltage-gated, transient outward current (I_{TO}), which is a major repolarizing potassium current in ovine atrial cells.[301,302] The analysis of SA effects focused on peak I_{TO} and the steady-state current (I_{SS}). Compared to control, SA significantly reduced I_{TO} density, which was measured at voltages in the range of -40 mV to +60 mV (Figure 3.3.3G & H). At +40 mV for example, there was a

~30% reduction of current density from 4.1 ± 0.6 pA/pF to 2.6 ± 0.3 pA/pF (*p<0.05). However, the SA incubation did not change I_{SS} density (Figure 3.3.3I).

3.3.4 Human atrial action potential simulations

Our results on the SA induced inhibition of I_{CaL} and I_{TO} are expected to differentially modulate atrial cell action potential, by an abbreviation (I_{CaL}), or a prolongation (I_{TO}), of APD. Although the current density measurements (Figure 3.3.3) would suggest a predominant effect of the former, it was not possible in the experiments to determine whether the SA effects on these ionic mechanisms were sufficient to explain the abbreviation, or whether other (ionic) mechanisms were necessary. Numerical simulations were therefore used to further investigate these possibilities. We incorporated the experimental results (of Figure 3.3.3) into a previously published human atrial cell model.[303] Currents in the presence of SA were introduced in the simulations by decreasing peak $I_{Ca\text{-}L}$ (by 60%) and I_{TO} (by 30%) compared to their respective control values. The model-generated action potentials, under control and with SA treatment, are shown respectively in the left and right panels of Figure 3.3.4. Results from the simulations showed that these changes in ionic current densities were sufficient to reproduce the reduced APD values (APD30, APD50 and APD80) measured experimentally. For example, control APD80 was reduced from 188.6 ± 7.7 msec to 82 ± 0.7 msec. Our simulation results are thus consistent with the results of our cell electrophysiology experiments in isolated atrial myocytes.